Electronic Supporting Information for:

Synthesis, characterization, and theoretical analysis of a plutonyl phosphine oxide complex

Cory J. Windorff,[a,b] * Maria J. Beltran-Leiva,[a] Thomas E. Albrecht-Schönzart,[a] Zhuanling Bai,[a] Cristian Cellis-Barros,[a]* Conrad A. P. Goodwin,[c,d] Zachary Huffman,[a] Noah C. McKinnon,[a] and Joseph M. Sperling,[a]

[a]Department of Chemistry and Biochemistry, Florida State University, 95 Chieftan Way, RM. 118 DLC, Tallahassee, Florida 32306, United States.

[b]Department of Chemistry and Biochemistry, New Mexico State University, MSC 3C, PO Box 3001, Las Cruces, NM 88003, United States.

[c]Chemistry Division, Los Alamos National Laboratory, Los Alamos, NM 87545, United States.

[d]Current Address: Department of Chemistry, School of Natural Sciences, The University of Manchester, Oxford Road, Manchester, M13 9PL, United Kingdom.

*To whom correspondence should be addressed: windorff@nmsu.edu; ccelisbarros@fsu.edu

TABLE OF CONTENTS **PAGE**

EXPERIMENTAL DETAILS, UV-VIS-NIR, AND MULTI-NUCLEAR NMR SPECTRA

Caution! *^{239}Pu ($t_{1/2}$ = 24,100 years) and its daughters have high specific activity α-particle and γ-ray emitting radionuclides. Its use presents extreme hazards to human health. This research was conducted in radiological a facility with appropriate analyses of these hazards, implementing controls for the safe handling and manipulation of these toxic and radioactive materials.*

Caution! *Ozone is a strongly oxidizing gas which reacts violently with nitrates and some organic molecules. Ozone was plumbed directly into a well-ventilated fume hood using PTFE tubing. Care was taken to minimize exposure to ozone. Once the reaction was set up the area was closed off until completion of the reaction. Pure O_2 was allowed to purge the system for 5 min once the ozone generator was turned off.*

Materials. All manipulations were conducted in air with no attempt to exclude air or water. The following solvents and reagents were purchased from commercial sources and used as received: Acetone (Sigma), MeOH (Sigma), EtOH (Sigma), ether (stabilized, VWR), CH_2Cl_2 (Stabilized, Sigma), HCl (concentrated, Sigma), $HClO_4$ (concentrated, Sigma), $CDCl_3$ (Cambridge) CD_2Cl_2 (Cambridge), $OPcy_3$ (cy = cyclohexyl, C_6H_{11}, Alpha Aesar), $OPPh_3$ (Sigma), $UO_2(NO_3)_2$•$6H_2O$ (Sigma), UO_3•$2H_2O$ (Strem), ^{239}Pu (Los Alamos National Lab) was prepared as a stock solution in HCl (2 M), O_2 (air gas), and 18 MΩ water was obtained from a Millipore purification system. Ozone was generated using pure oxygen using an Ozonology ozone generator at 100% voltage with an initial flow rate of 8 SCFH which was decreased to a flow rate of 4 SCFH for standing overnight. Ozone test strips were used to confirm the initial presence of O_3 bubbled into water. $^{239}PuO_2Cl_2$•nH_2O was prepared by gently bubbling a stream of $O_{3(g)}$ into a blue solution of $^{239}PuCl_3(H_2O)_x$ in HCl (~5 mL, 2 M) overnight (c.a. 17 h) over which time the solution had gone to dryness. The brown residue was dissolved in a known amount of H_2O instantly producing a pink solution and a small sample was spiked into $HClO_4$ (1 M) for UV-vis-NIR confirmation of oxidation state purity, see below for spectrum, the aqueous solution was then evaporated under a stream of nitrogen to give a brown residue formulated as $^{239}PuO_2Cl_2(H_2O)_x$ used in the reaction. UO_2Cl_2•$3H_2O$ was synthesized by dissolution of UO_3•nH_2O in HCl (concentrated) and evaporated to a residue under a stream of nitrogen, stored in a desiccator and used with the assumption that n = 3. $UO_2Cl_2(OPPh_3)_2$, **2-U**, and $UO_2(NO_3)_2(OPPh_3)_2$, **4-U**, were synthesized according to the literature, by carefully layering $OPPh_3$ in EtOH or acetone on a solution of UO_2X_2•nH_2O (X = Cl, NO_3) in EtOH or

acetone, respectively, at room temperature, giving X-ray quality crystals overnight.[1, 2] The observed NMR spectra of $UO_2(NO_3)_2(OPPh_3)_2$, **4-U**, differs slightly from the literature and is given herein.[3] The solubility of $UO_2Cl_2(OPPh_3)_2$, **2-U**, proved to be too low in $CDCl_3$ to obtain a useable spectrum but we note that there are several studies on the electronic spectroscopy of $UO_2X_2(OPPh_3)_2$ (X = Cl, NO_3) compound.[4-7]

Instrumentation. **NMR Spectroscopy:** ^{1}H, $^{13}C\{^{1}H\}$, and $^{31}P\{^{1}H\}$ NMR spectra of uranium compounds were recorded on a Bruker 600 MHz spectrometer operating at 600.13, 150.90, and 242.94 MHz, respectively, at 298 K, spectra of plutonium compounds were collected on a Bruker 400 MHz spectrometer operating at 400.17, 100.62, and 161.99 MHZ, respectively at 298 K, unless otherwise stated. ^{1}H and $^{13}C\{^{1}H\}$ NMR spectra were referenced internally to solvent resonances[8] and $^{31}P\{^{1}H\}$ spectra were referenced externally to 85% H_3PO_4. For radiological containment $PuO_2Cl_2(OPcy_3)_2$, **1-Pu**, was partially dissolved in $CDCl_3$, carefully transferred to a Teflon® NMR tube liner, checked for contamination, placed in a high quality borosilicate NMR tube, capped, placed in a Ziplock® bag and transported to the NMR spectrometer. **UV-vis-NIR Spectroscopy:** Solution phase UV-vis-NIR spectroscopic data were obtained using an Agilent Technologies Cary series 6000i UV/vis/NIR spectrophotometer. Samples were dissolved and placed in a 1 cm small volume quartz cell, plutonium samples were prepared by wrapping the cuvette in parafilm, to reduce contamination, and the cuvette was checked for contamination before recording spectra. Solid state UV-vis-NIR spectroscopic data were obtained from single crystals using a CRAIC Technologies UV-vis-NIR microspectrophotometer. Crystals were placed on glass slides in immersion oil and data were collected from 300 nm to 1700 nm. **High Resolution MS:** High resolution mass-spectra were recorded on uranium samples using an Agilent 6200 Q-TOF-MS coupled to a DART SVP (IonSense) ambient ionization source. All analyses were conducted in positive mode with a DART helium gas at 350 °C, Q-TOF heater gas (He) at 300 °C, drying gas flow at 0.2 L/min, fragmentor voltage 175 V, skimmer voltage 65 V, and a mass range of 100-1700 amu with high resolution. Due to radiologic hazards, it was not possible to perform DART-MS on samples containing plutonium complexes. **X-ray Crystallography:** Single crystals selected for data collection were mounted on a MITOGEN mount™ cryoloop and optically aligned on a Bruker D8 Quest X-ray diffractometer. Crystallographic data was collected low-temperature nitrogen gas flow using a Mo-K_α (λ = 0.71069 Å) IμX-ray micro source and a CMOS detector. The unit cell determination and subsequent data collection was performed using the APEX III program package.[9] The raw data was imported into CrysAlisPro

using the SAXI "creatrunlist" command.[10] Data reduction and absorption correction by the multi-scan method were performed using CrysAlisPro. The structure was solved by intrinsic phasing with ShelXT[11] and refined on F^2 by full-matrix least-squares techniques with ShelXL.[12] The analytical scattering factors for neutral atoms were used throughout the analysis.[13] Hydrogen atoms were included using a riding model. Full details on crystallographic refinement and experiments can be found in the Crystallographic Details section. Crystallographic information files for the complexes are available for free through the Cambridge Crystallographic Data Centre (CCDC).

Theoretical Details. All of the actinyl systems were analyzed through density functional theory (DFT) and the complete active space self-consistent field (CASSCF). Kohn-Sham (KS) DFT orbitals were used as starting point for CASSCF calculations. For KS-DFT calculations, the PBE0[14] functional in conjunction with the def2-TZVP basis set,[15] were used for all atoms except plutonium and uranium, which were treated with the SARC-DKH-TZVP basis set.[16] Scalar relativistic effects were included via the second-order Douglas-Kroll-Hess (DKH2) Hamiltonian.[17] In order to keep the solid-state geometry of $UO_2Cl_2(OPcy_3)_2$, **1-U**, and $PuO_2Cl_2(OPcy_3)_2$, **1-Pu**, no geometry optimizations were performed. The theoretical model of the $(UO_2)^{2+}$ and $(PuO_2)^{2+}$ ions were optimized in ADF2019 using the hybrid PBE0 functional along with the STO-TZP basis set.[18] Scalar relativistic effects in ADF were included using the ZORA Hamiltonian which is well-known to yield similar results to DKH2.[19] The resulting wavefunctions were used to carry out state average CASSCF calculations that allowed us to recover static, and some dynamic correlation energy.[20] The active space consisted of *n* electrons in 10 orbitals, CAS(*n*,10), including seven 5*f* and 3 additional orbitals ($1 \times p_\sigma$ and $2 \times p_\pi$) to consider the interaction between the metal center and the axial oxygen atoms (n = 6, 8 for U and Pu, respectively). Scalar relativistic effects were incorporated by the DKH2 Hamiltonian, while spin-orbit (SO) coupling by quasi-degenerate perturbation theory (QDPT). A more accurate treatment of dynamic correlation was achieved by N-electron valence state perturbation theory (NEVPT2), where excitations outside the active space are also considered.[21] All these calculations were carried out using the ORCA 4.2.1 package.[22]

The interaction between uranium and plutonium with the environment was analyzed by the Quantum Theory of Atoms in Molecules (QTAIM).[23] To gain insight into the chemical bond, the electron density, $\rho(r)$, delocalization, $\delta(r)$, localization, $\lambda(M)$ indices, and energy densities: potential, V(r), kinetic, G(r), and total energy H(r), densities were analyzed. The AIMAII

software was used to perform QTAIM calculations based on CASSCF wavefunctions.[24] The chemical bond was further analyzed by means of the Natural Bond Orbital (NBO) theory using the scalar relativistic CASSCF wavefunctions.[25, 26] The NBO7.0 software was used to perform the analysis.[27]

Synthesis of Compounds.

$^{239}PuO_2Cl_2(OPcy_3)_2$, 1-Pu. As an alternative to the literature,[28] EtOH (250 μL) was carefully pipetted through a 1.00 mL pipette tip placed above a colorless EtOH (1.00 mL) solution of $OPcy_3$ (40 mg, 130 μmol) in a 6 mL scintillation vial. Then a brown solution of $PuO_2Cl_2(H_2O)_x$ (ca. 17 mg of ^{239}Pu content, 60 μmol) in MeOH (500 μL) was carefully pipetted through the same 1.00 mL pipette tip to layer the Pu solution on top of the ligand solution. The 1.00 mL pipette tip was washed with EtOH (1 × 250 μL) to remove small droplets remaining on the pipette tip. The vial was loosely capped and left undisturbed. After ca. 4 hours small yellow/brown X-ray quality crystals and some amorphous powder was observed at the bottom of the vial. A sample was drawn for X-ray crystallography and solid-state UV-vis-NIR spectroscopy by carefully tilting the scintillation vial to expose a few crystals. Crystals were retrieved using a melting point capillary with a small amount of immersion oil on the sealed end. This was repeated several times to achieve a reasonable sample size. The analyses confirmed the synthesis of **1-Pu**. The next day following confirmation of the product the solvent was allowed to evaporate in the fume hood and the yellow solids were washed with ether (3 × 0.75 mL) dried in air (ca. 1 hr) and brought into a glovebox dedicated to transuranium chemistry giving $PuO_2Cl_2(OPcy_3)_2$ (60 mg, 90%) as a yellow solid. The yield was determined based on Pu-element content, assuming purity by ^{31}P NMR spectroscopy. *Due to the paramagnetism of $(PuO_2)^{2+}$ ($5f^2$), only unambiguously identifiable resonances are assigned, copies of the spectra are given below*. ^{1}H NMR ($CDCl_3$; 400 MHz, 295 K) δ: 1.70 to –0.36 (multiple broad overlapping resonances), –3.61 (s, 12H, *cy*), –14.71 (s, 12H, *cy*), –16.03 (s, 12H, *cy*), –25.26 (s, 6H, *cy*); $^{13}C\{^1H\}$ NMR ($CDCl_3$; 101 MHz, 295 K) δ: 25.17, 24.90, 22.77, 22.32, 19.6, 7.18, 6.71; $^{31}P\{^1H\}$ NMR ($CDCl_3$; 162 MHz, 295 K) δ: –5.57, –110.97 . UV-vis-NIR (single crystal λ_{max}, nm, [cm^{-1}]): 765 [13,100], 824[12,150], 828 [12,100], 883 [11,300], 895 [11,200], 905 [11,050], 917 [10,100], 977 [10,200], 992 [10,100].

Table S1. Vertical excitation energies of $(PuO_2)^{2+}$ and **1-Pu** obtained from spin-orbit CASSCF wavefunctions corrected by perturbation theory (SO-PT2) from the ^3H_g ground state, which features a $p_\pi^4 p_\sigma^2 f_\varphi^1 f_\delta^1 f_\pi^0 f_\sigma^0$ configuration. The composition and assignment of each excited state is given in terms of contributions to spin-free states given in parenthesis. For clarity the filled and empty $p_\pi^4 p_\sigma^2$and $f_\pi^0 f_\sigma^0$ orbitals, respectively, are part of all the configurations described below, have been omitted.

SO-State	Energy (cm^{-1}) & Contribution		$(PuO_2)^{2+}$	SO-State	Energy (cm^{-1}) & Contribution		1-Pu
4_g	0	96%	$f_\delta^1 f_\varphi^1$ (^3H_g)	**4_g**	0	92%	$f_\delta^1 f_\varphi^1$ (^3H_g)
		4%	$f_\delta^2 f_\varphi^0$ ($^1\Gamma_g$)			6%	$f_\delta^2 f_\varphi^0$ ($^1\Gamma_g$)
0^+_g	3097.4	54%	$f_\delta^2 f_\varphi^2$ ($^3\Sigma^-_g$)*	**0^+_g**	2707.5	60%	$f_\delta^2 f_\varphi^2$ ($^3\Sigma^-_g$)*
		20%	$f_\delta^1 f_\varphi^1$ ($^3\Pi_g$)			25%	$f_\delta^1 f_\varphi^1$ ($^3\Pi_g$)
		14%	$f_\delta^2 f_\varphi^2$ ($^1\Sigma^+_g$)			13%	$f_\delta^2 f_\varphi^2$ ($^1\Sigma^+_g$)
1_g	5518.9	49%	$f_\delta^1 f_\varphi^1$ ($^3\Pi_g$)	**1_g**	4672.4	43%	$f_\delta^1 f_\varphi^1$ ($^3\Pi_g$)
		28%	$f_\delta^2 f_\varphi^2$ ($^3\Sigma^-_g$)			40%	$f_\delta^2 f_\varphi^2$ ($^3\Sigma^-_g$)
		15%	$f_\delta^1 f_\varphi^1$ ($^1\Pi_g$)			11%	$f_\delta^1 f_\varphi^1$ ($^1\Pi_g$)
5_g	6803.9	100%	$f_\delta^1 f_\varphi^1$ (^3H_g)	**5_g**	7198.6	100%	$f_\delta^1 f_\varphi^1$ (^3H_g)
0^-_g	10,618.1	100%	$f_\delta^1 f_\varphi^1$ ($^3\Pi_g$)	**0^-_g**	10,713.53	100%	$f_\delta^1 f_\varphi^1$ ($^3\Pi_g$)
1_g	11,156.9	63%	$f_\delta^2 f_\varphi^2$ ($^3\Sigma^-_g$)	**1_g**	10,962.5	56%	$f_\delta^2 f_\varphi^2$ ($^3\Sigma^-_g$)
		11%	$f_\delta^1 f_\varphi^1$ ($^3\Pi_g$)			20%	$f_\delta^1 f_\varphi^1$ ($^3\Pi_g$)
		20%	$f_\delta^1 f_\varphi^1$ ($^1\Pi_g$)			20%	$f_\delta^1 f_\varphi^1$ ($^1\Pi_g$)
0^+_g	12,161.7	60%	$f_\delta^1 f_\varphi^1$ ($^3\Pi_g$)	**0^+_g**	11,981.7	62%	$f_\delta^1 f_\varphi^1$ ($^3\Pi_g$)
		12%	$f_\delta^2 f_\varphi^2$ ($^3\Sigma^-_g$)			7%	$f_\delta^2 f_\varphi^2$ ($^3\Sigma^-_g$)
		27%	$f_\delta^2 f_\varphi^2$ ($^1\Sigma^+_g$)			25%	$f_\delta^2 f_\varphi^2$ ($^1\Sigma^+_g$)
6_g	12,218.4	88%	$f_\delta^1 f_\varphi^1$ (^3H_g)	**6_g**	12,469.4	92%	$f_\delta^1 f_\varphi^1$ (^3H_g)
		7%	$f_\delta^0 f_\varphi^2$ (^1I_g)				
2_g	12,762.8	94%	$f_\delta^1 f_\varphi^1$ ($^3\Pi_g$)	**2_g**	12,938.4	92%	$f_\delta^1 f_\varphi^1$ ($^3\Pi_g$)

*The $^3\Sigma^-_g$ spin-free state has equal contribution from $f_\delta^2 f_\varphi^0$ and $f_\delta^0 f_\varphi^2$ configurations, for simplicity the notation is written as $f_\delta^2 f_\varphi^2$.

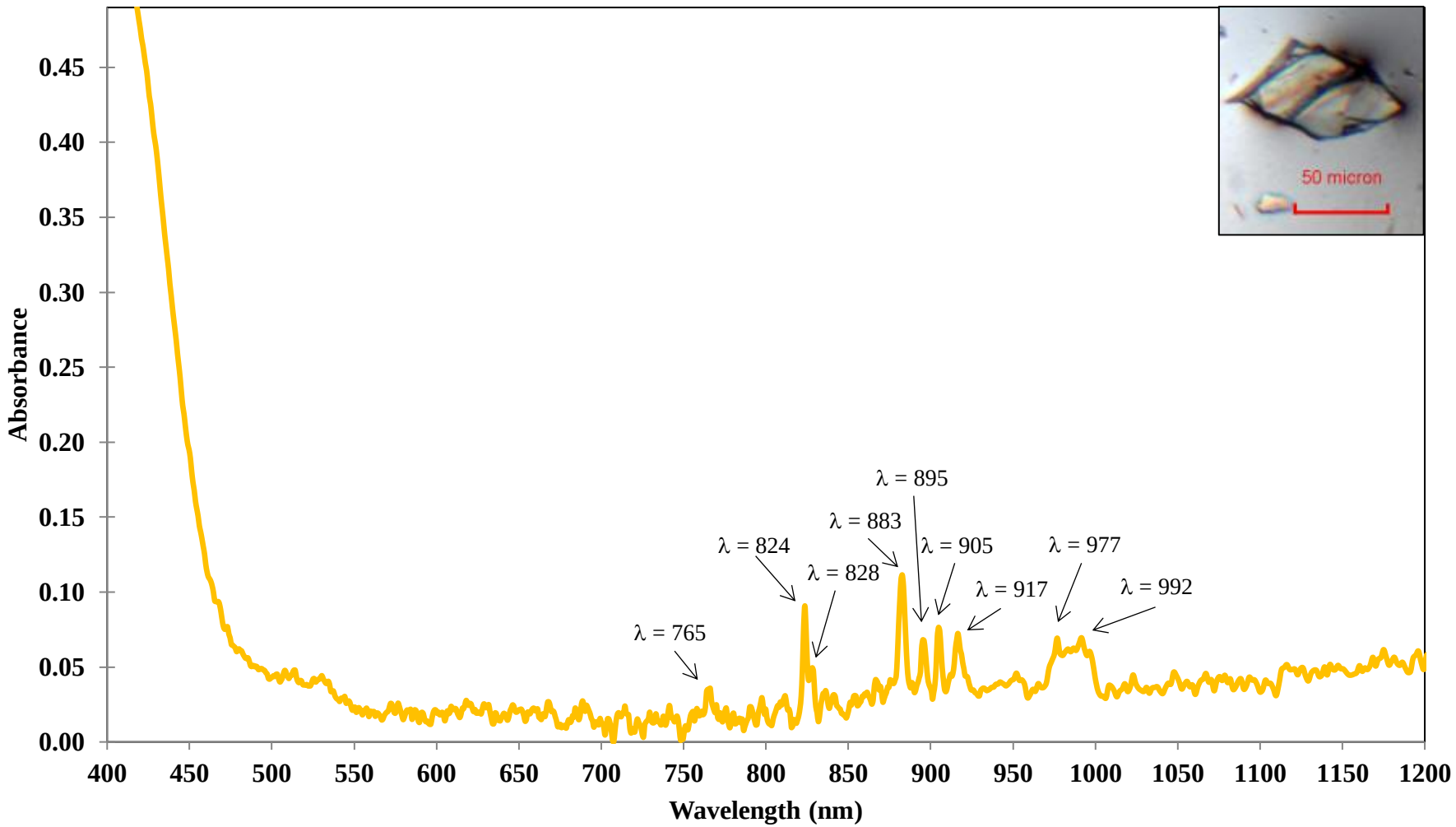

Figure S1. Solid state UV-vis-NIR spectrum, plotted in wavelength (nm), of $PuO_2Cl_2(OPcy_3)_2$, **1-Pu**, at ambient temperature with photograph of isolated crystal sample.

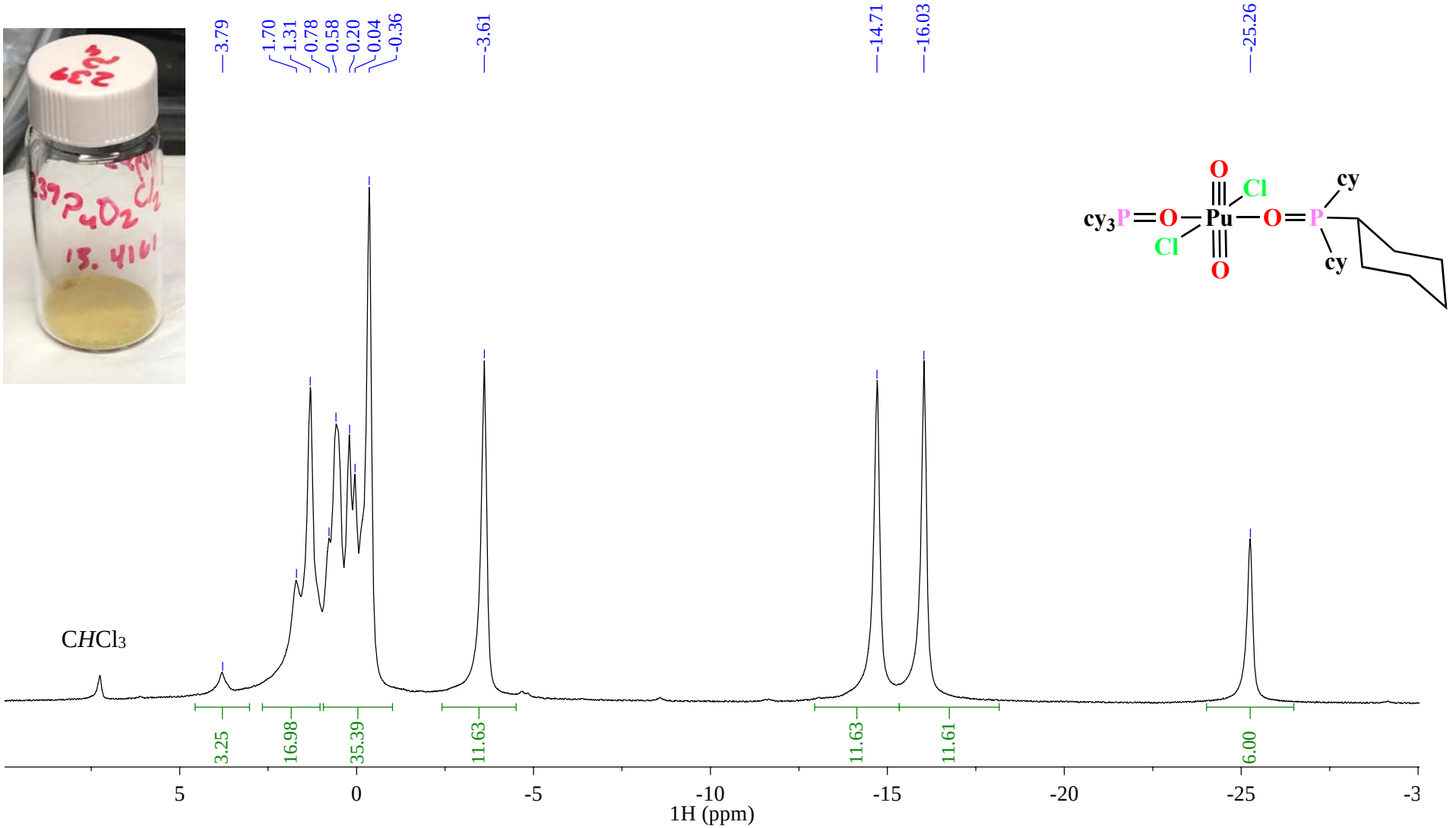

Figure S2. ^{1}H NMR spectrum of $PuO_2Cl_2(OPcy_3)_2$, **1-Pu**, in $CDCl_3$ at ambient temperature with photograph of bulk sample.

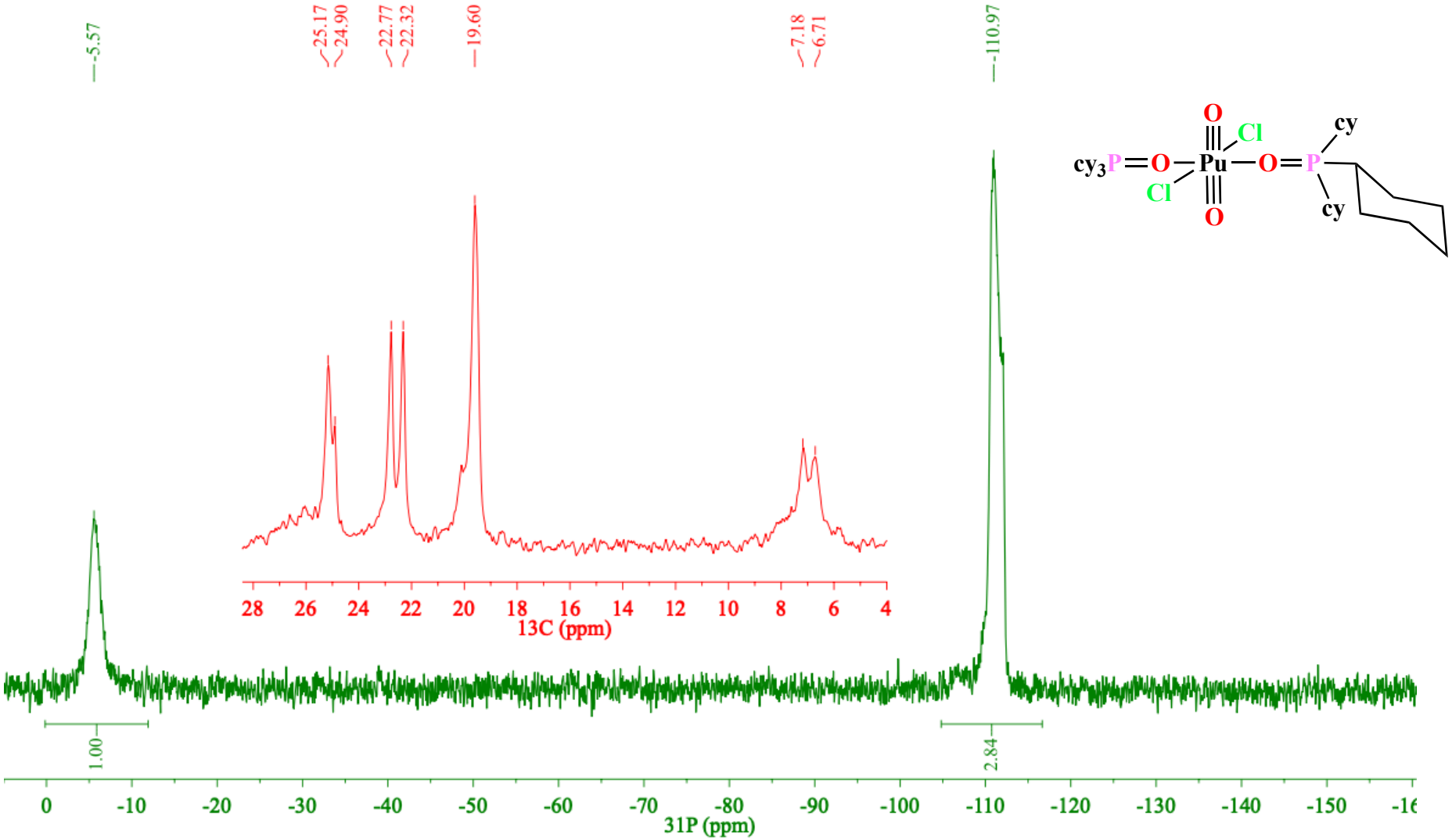

Figure S3. $^{31}P\{^{1}H\}$ (green) and $^{13}C\{^{1}H\}$ (red, inset) NMR spectra of $PuO_2Cl_2(OPcy_3)_2$, **1-Pu**, in $CDCl_3$ at ambient temperature processed with a 7 Hz line broadening and relative ^{31}P NMR integrations.

After ca. 1 month solid $OPcy_3$ (15 mg, 50 μmol) was added in several portions to the NMR spectroscopic sample of $PuO_2(OPcy_3)_2$ in $CDCl_3$, that had been in solution during the month, an initial red color formed (characteristic of Pu^{4+}), and dissipated as the solution mixed. The NMR tube was resealed and reanalyzed, and a solution phase UV-vis-NIR spectrum was recorded. *Due to the evidence of free $OPcy_3$, the paramagnetism of $(PuO_2)^{2+}$ ($5f^2$), and the evidence of Pu^{4+} ions ($5f^4$), which are typically paramagnetic, only unambiguously identifiable resonances are assigned, see below for spectra*. ^{1}H NMR ($CDCl_3$; 400 MHz, 295 K) δ: 1.67 to –0.43 (multiple peaks), –3.69 (s, 6H, *cy*). –14.82 (s, 6H, *cy*), –16.16 (s, 6H, *cy*), –25.38 (s, 3H, *cy*); ^{31}P{^{1}H} NMR ($CDCl_3$; 162 MHz, 295 K) δ: 57.70, 55.37 (free $OPcy_3$ and putative Pu^{4+}–$OPcy_3$ complex), –6.27, –112.49. UV-vis-NIR ($CDCl_3$, λ_{max}, nm [cm^{-1}]):[29] <300–435 [>33,300–23,000] (broad charge transfer), 512 [19,500], 530 [18,900], 623 [16,050], 659 [15,200], 680 [14,700], 720 [13,900], 780 [12,800], 792 [12,600], 820 [12,200], 830 [12,050], 879 [11,400], 971 [10,300], 996 [10,050], 1027 [9,750], 1084 [9,225], 1103 [9,075], 1200 [8,330], 1376 [7,270], 1383 [7,230], 1431 [6,990], 1434 [6,970], 1439 [6,950], 1441 [6,940], 1470 [6,800], 1495 [6,690], 1585 [6,310], 1722 [5,810], 1750 [5,710].

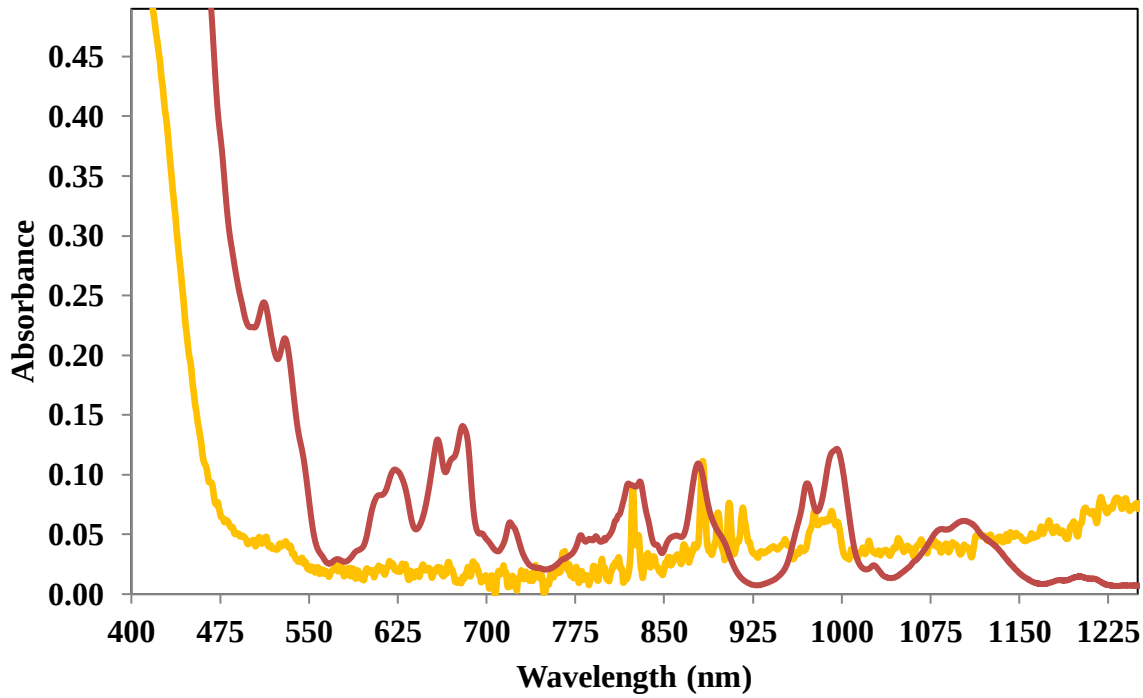

Figure S4. Comparison of solid-state spectrum of fresh $PuO_2Cl_2(OPcy_3)_2$, **1-Pu**, (yellow trace) and solution phase spectrum of **1-Pu** after standing in $CDCl_3$ for one month (red trace).

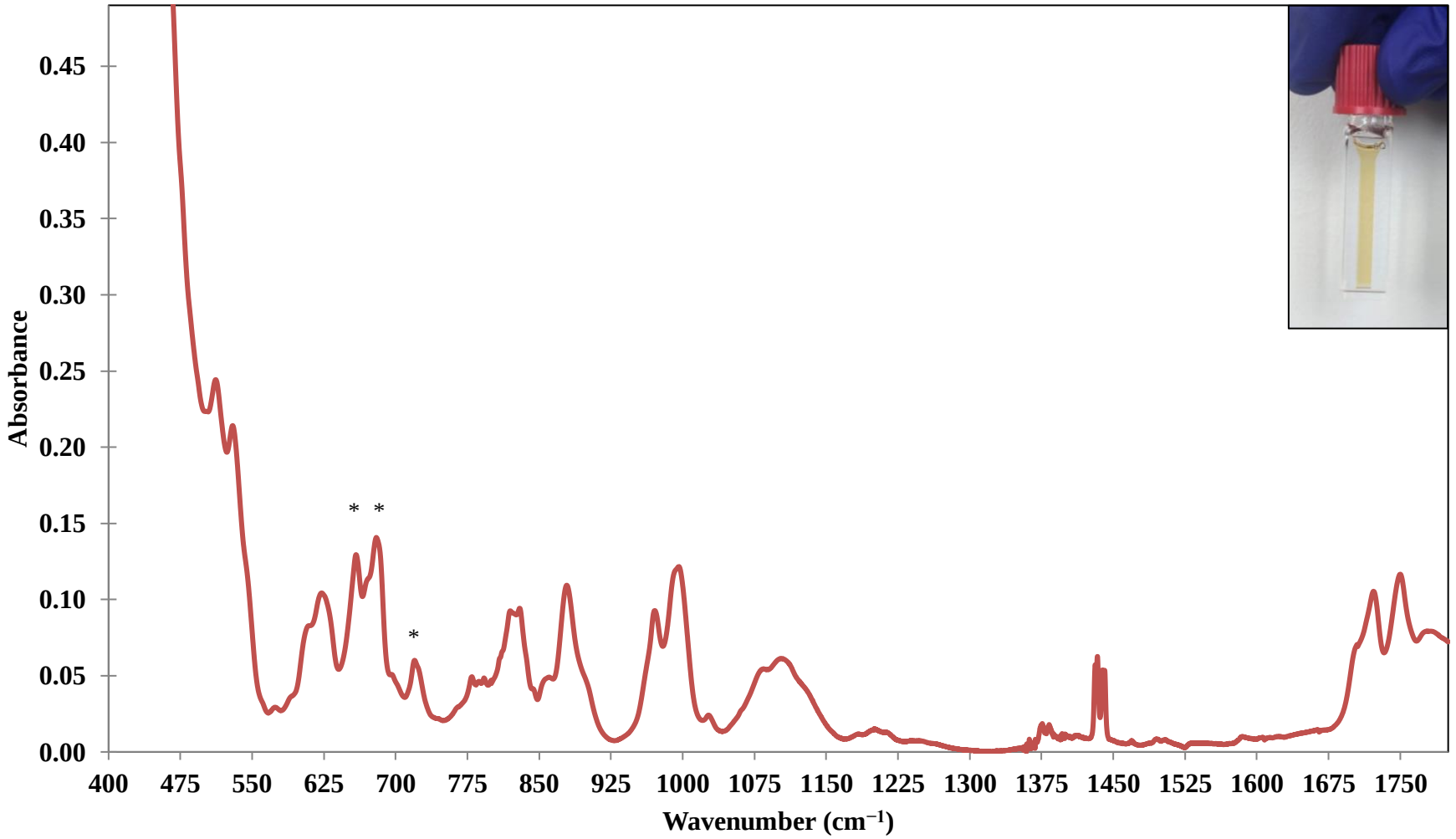

Figure S5. Solution phase UV-vis-NIR spectrum, plotted in wavelength (nm), of $PuO_2Cl_2(OPcy_3)_2$, **1-Pu**, in $CDCl_3$ after sitting one month at ambient temperature, with photograph of sample. *Denotes characteristic Pu(IV) excitations.

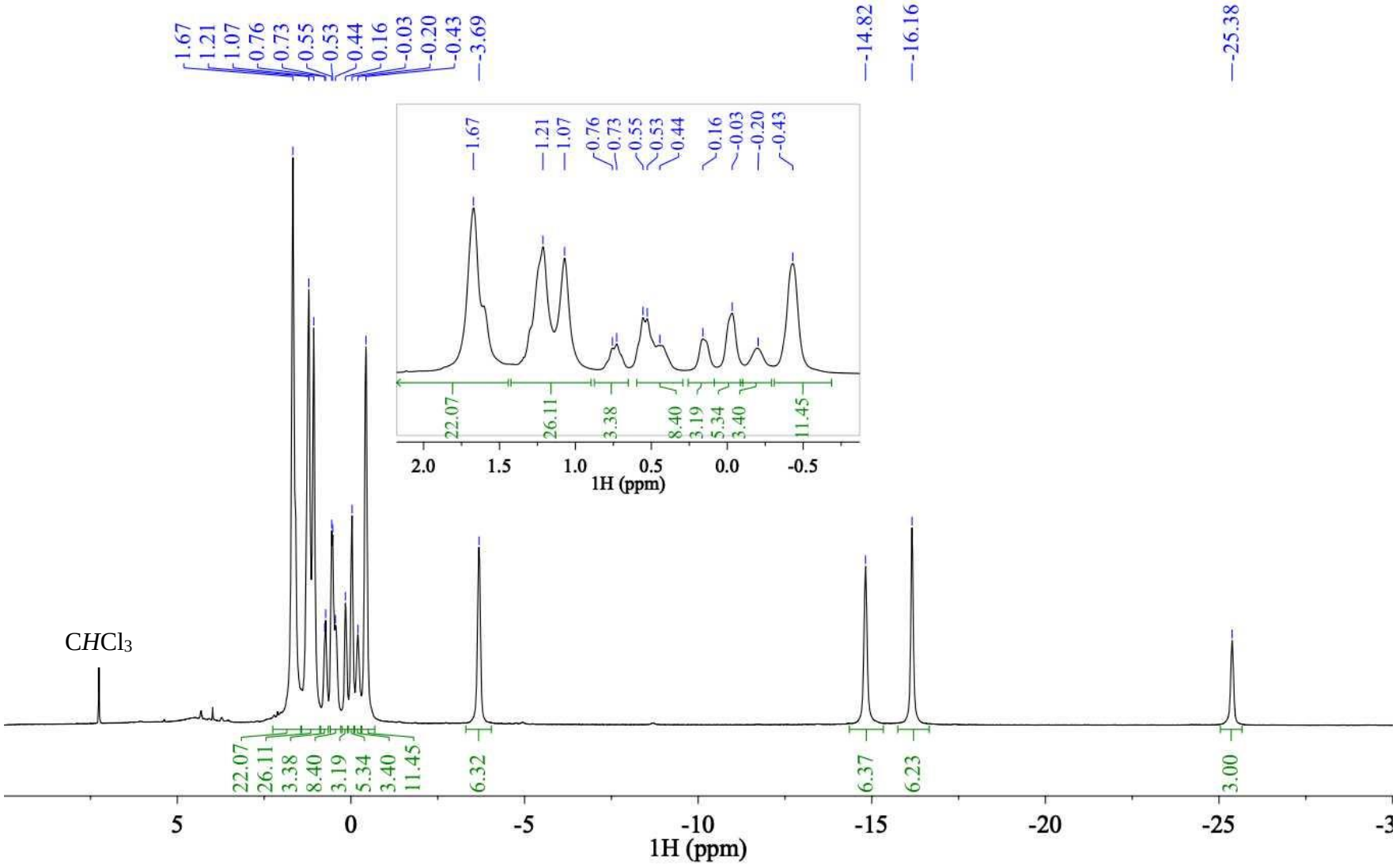

Figure S6. ^{1}H NMR spectrum of $PuO_2Cl_2(OPcy_3)_2$, **1-Pu**, with inset of 2.25 to –0.75 ppm region, in $CDCl_3$ recorded after one month of standing at room temperature and additional $OPcy_3$ added. The integrations are relative to a single $OPcy_3$ molecule.

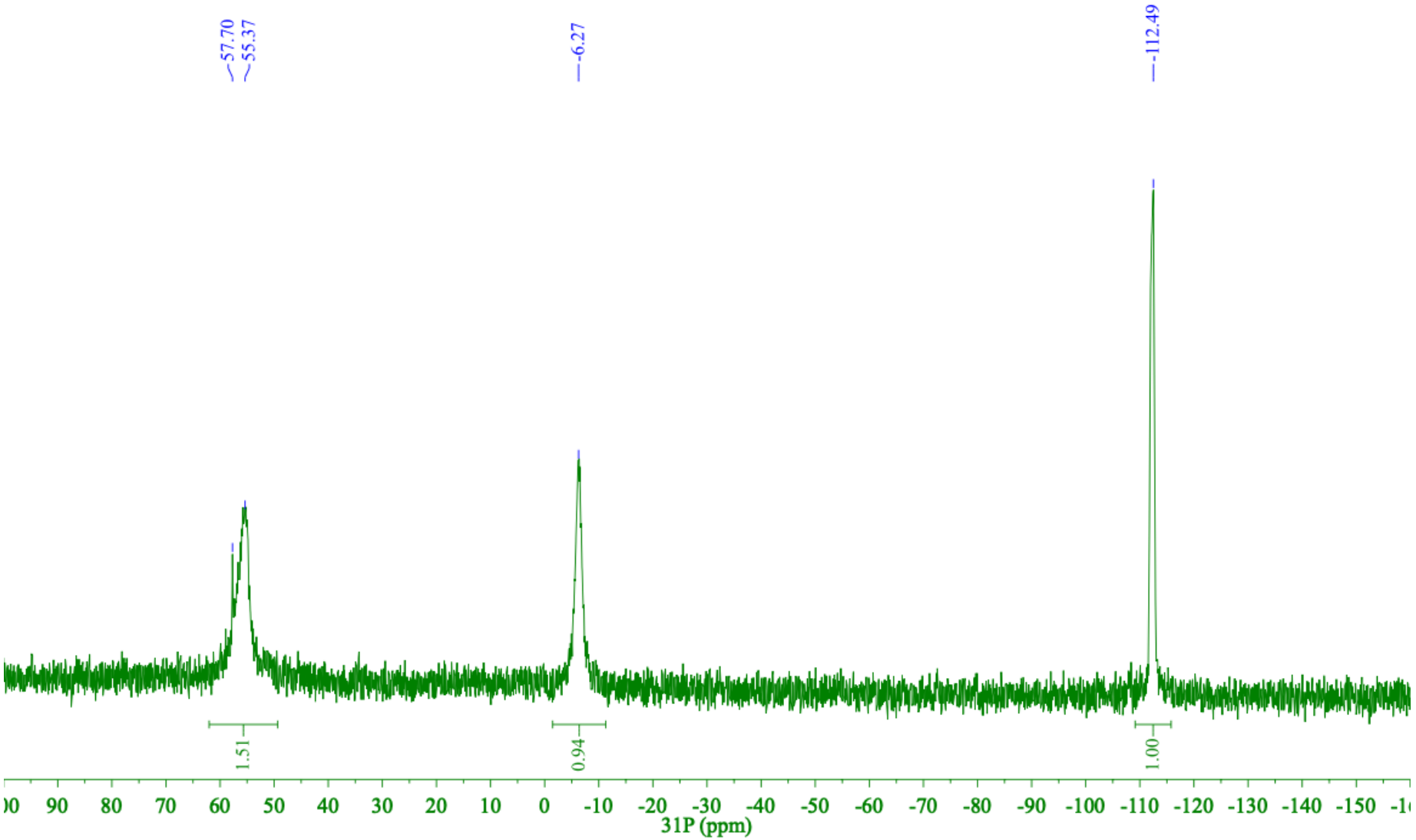

Figure S7. $^{31}P\{^{1}H\}$ NMR spectrum of $PuO_2Cl_2(OPcy_3)_2$, **1-Pu**, in $CDCl_3$ recorded after one month of standing at room temperature and additional $OPcy_3$ added, processed with 5 Hz line broadening.

$UO_2Cl_2(OPcy_3)_2$, 1-U. As an alternative to the literature,[30] a solution of $OPcy_3$ (40 mg, 130 μmol) in EtOH (1.00 mL) was added to a bright yellow solution of $UO_2Cl_2 \cdot 3H_2O$ (26 mg, 65 μmol) in EtOH (1.50 mL) in a 6 mL scintillation vial. The vial was caped and left undisturbed overnight producing X-ray quality crystals. A small sample was drawn for X-ray crystallography, the colorless mother liquor was decanted, washed with ether (3 × 1 mL), and dried in air to give **1-U** as a bright yellow solid (40 mg, 66%). The $^{31}P\{^1H\}$ NMR spectrum in CD_2Cl_2 was consistent with the published spectrum.[30] UV-vis-NIR (DCM, λ_{max}, nm, [cm^{-1}], (ε, $M^{-1}cm^{-1}$)): ~220–330 [45,500–30,300] (>80, broad charge transfer band), 358 [27,900] (3, sh), 372 [26,900] (2), 381 [26,200] (2), 389 [25,700] (2), 400 [25,000] (2), 403 [24,800] (2), 412 [24,250] (4), 415 [24,100] (4), 424 [23,600] (5), 427 [23,400] (5), 436 [22,925] (4), 440 [22,700] (5), 454 [22,000] (2), 463 [21,575] (1), 473 [21,150] (1), 479 [20,875] (1), 489 [20,450] (1), 496 [20,150] (1), 504 [19,825] (1).

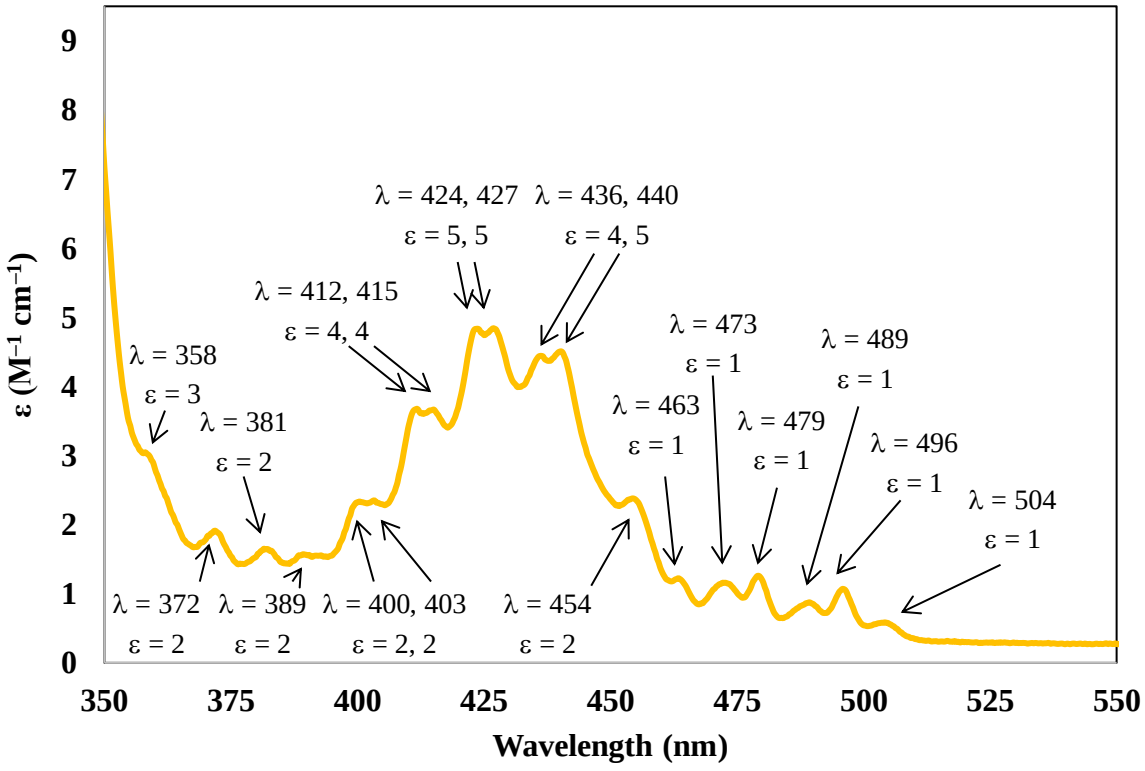

Figure S8. Solution phase UV-vis-NIR spectrum of $UO_2Cl_2(OPcy_3)_2$, **1-U,** plotted in units of wavelength (nm), in DCM recorded at ambient temperature.

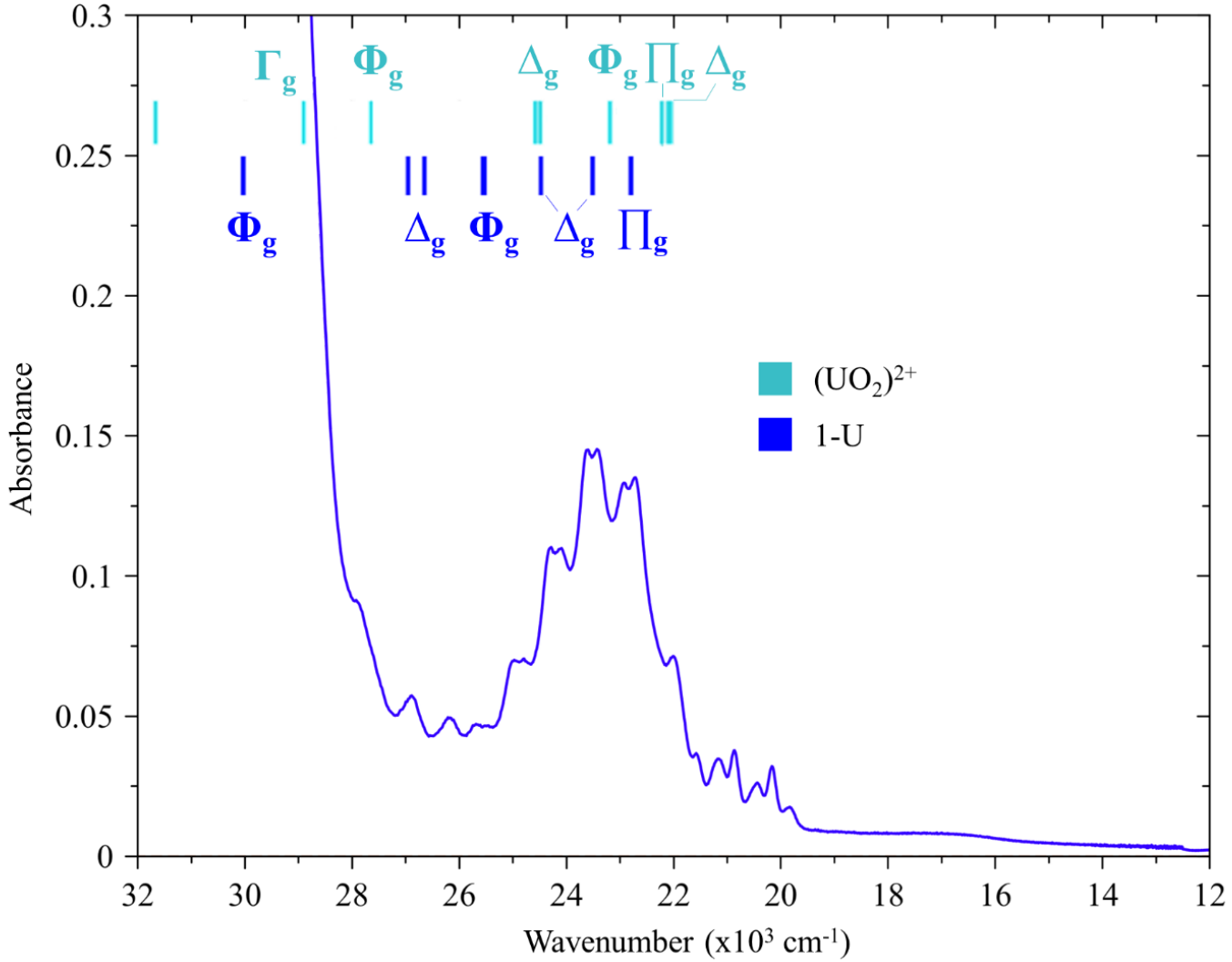

Figure S9. Solution phase UV-vis-NIR spectra of $UO_2Cl_2(OPcy_3)_2$, **1-U** recorded at ambient temperature in DCM plotted in units of energy (cm^{-1}) with SO-PT2 states of **3** and $(UO_2)^{2+}$ included to gain more insight in the assignment of the bands.

Table S2. Vertical excitation energies of $(UO_2)^{2+}$ and **1-U** obtained from spin-orbit CASSCF wavefunctions corrected by perturbation theory (SO-PT2) from the $^1\Sigma_g$ ground state, which features a $p_\pi^4 p_\sigma^2 f_\varphi^0 f_\delta^0 f_\pi^0 f_\sigma^0$ configuration. The composition and assignment of each excited state is given in terms of contributions of spin-free states, given in parenthesis. For clarity the filled and empty $p_\pi^4 p_\sigma^1$and $f_\pi^0 f_\sigma^0$ orbitals, respectively, are part of all the configurations described below, have been omitted.

SO-State	**Energy (cm^{-1}) & Contribution**		**$(UO_2)^{2+}$**	**SO-State**	**Energy (cm^{-1}) & Contribution**		**1-U**
Δ_g	22087.3	64%	$f_\varphi^1 f_\delta^0$ ($^3\Phi_g$)	Π_g	22863.4	90%	$f_\delta^1 f_\varphi^0$ ($^3\Delta_g$)
		34%	$f_\varphi^0 f_\delta^1$ ($^3\Delta_g$)				
Π_g	22210.5	97%	$f_\varphi^0 f_\delta^1$ ($^3\Delta_g$)	Δ_g	24536.1	77%	$f_\delta^1 f_\varphi^0$ ($^3\Delta_g$)
						13%	$f_\delta^0 f_\varphi^1$ ($^3\Phi_g$)
Φ_g	23181.6	45%	$f_\varphi^1 f_\delta^0$ ($^3\Phi_g$)	Φ_g	25622.1	62%	$f_\delta^1 f_\varphi^0$ ($^3\Delta_g$)
		32%	$f_\varphi^0 f_\delta^1$ ($^3\Delta_g$)			16%	$f_\delta^0 f_\varphi^1$ ($^3\Phi_g$)
		13%	$f_\varphi^1 f_\delta^0$ ($^1\Phi_g$)			7%	$f_\delta^0 f_\varphi^1$ ($^1\Phi_g$)
Δ_g	24584	57%	$f_\varphi^0 f_\delta^1$ ($^3\Delta_g$)	Δ_g	27015.1	72%	$f_\delta^0 f_\varphi^1$ ($^3\Phi_g$)
		28%	$f_\varphi^1 f_\delta^0$ ($^3\Phi_g$)			7%	$f_\delta^1 f_\varphi^0$ ($^3\Delta_g$)
		10%	$f_\varphi^0 f_\delta^1$ ($^1\Delta_g$)			2%	$f_\delta^1 f_\varphi^0$ ($^1\Delta_g$)
Φ_g	27664.9	60%	$f_\varphi^0 f_\delta^1$ ($^3\Delta_g$)	Φ_g	30094.5	53%	$f_\delta^0 f_\varphi^1$ ($^3\Phi_g$)
		33%	$f_\varphi^1 f_\delta^0$ ($^3\Phi_g$)			28%	$f_\delta^1 f_\varphi^0$ ($^3\Delta_g$)
		3%	$f_\varphi^1 f_\delta^0$ ($^1\Phi_g$)			9%	$f_\delta^0 f_\varphi^1$ ($^1\Phi_g$)
Γ_g	28924.4	97%	$f_\varphi^1 f_\delta^0$ ($^3\Phi_g$)	Γ_g	32740.6	90%	$f_\delta^0 f_\varphi^1$ ($^3\Phi_g$)

$UO_2(NO_3)_2(OPcy_3)_2$, 3-U. A solution of $OPcy_3$ (29 mg, 100 μmol) in acetone (1.00 mL) was carefully layered on top of a yellow solution of $UO_2(NO_3)_2$•$6H_2O$ (25 mg, 49 μmol) in acetone (1.50 mL) in a 6 mL scintillation vial, some precipitation was observed immediately. The vial was capped and left undisturbed overnight, producing yellow X-ray quality crystals. A small sample was drawn for X-ray crystallography, the colorless mother liquor was decanted, washed with ether (3 × 1 mL), and dried in air to give **3-U** as a neon green/yellow solid (40 mg, 80%). ^{1}H NMR (CD_2Cl_2; 600 MHz) δ: 2.53 (q, J_{HH} = 12.3 Hz, 6H, *cy*), 2.22 (d, J_{HH} = 11.2 Hz, 12H, *cy*), 1.88 (d, J_{HH} = 10.6 Hz, 12H, *cy*), 1.74 (t, J_{HH} = 12.5 Hz, 18H, *cy*), 1.39 (q, J_{HH} = 12.8 Hz, 12H, *cy*), 1.23 (q. J_{HH} = 13.0 Hz, 6H, *cy*); ^{13}C{^{1}H} NMR (CD_2Cl_2; 151 MHz) δ: 35.82 (d, $^1J_{PC}$ = 59.5 Hz, ipso-*cy*), 27.21 (d, $^2J_{PC}$ = 12.4 Hz, *cy*) 26.36 (d, $^3J_{PC}$ = 2.9 Hz, *cy*), 26.32 (s, *cy*); ^{31}P{^{1}H} NMR (CD_2Cl_2; 243 MHz) δ: 48.61. UV-vis-NIR (DCM, λ_{max}, nm, [cm^{-1}], (ε, $M^{-1}cm^{-1}$)): ~240–310 [41,700–32,300] (>300, broad charge transfer band), 416 [24,000] (25), 427 [23,400] (27), 439 [22,800] (24), 454 [22,000] (14), 469 [21,300] (8), 485 [20,600] (3). DART-MS (m/z, relative abundance, %) = 924.56 (100), 925.56 (50) $[UO_2(NO_3)(OPcy_3)_2]^+$.

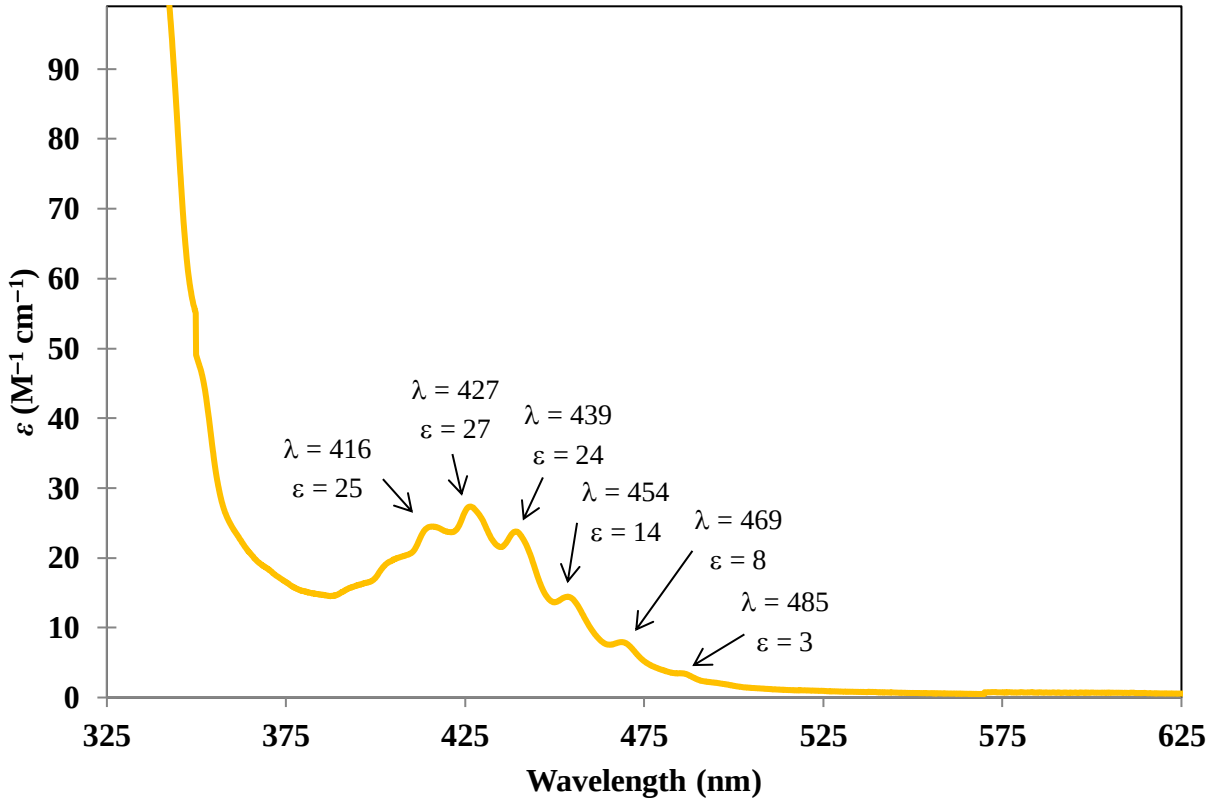

Figure S10. Solution phase UV-vis-NIR spectrum, of $UO_2(NO_3)_2(OPcy_3)_2$, **3-U** plotted in wavelength (nm), in DCM recorded at ambient temperature.

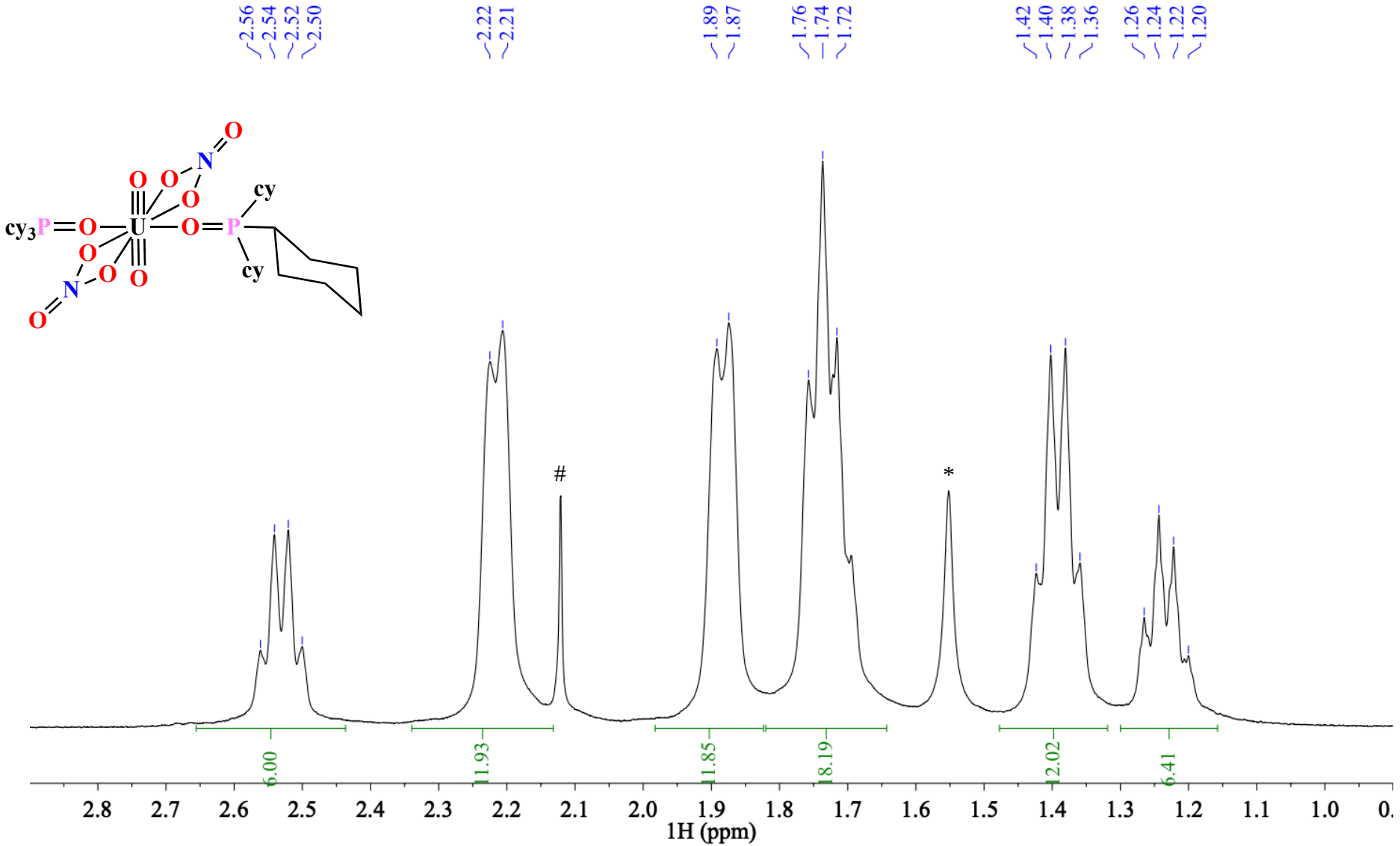

Figure S11. ^{1}H NMR spectrum of $UO_2(NO_3)_2(OPcy_3)_2$, **3-U**, in CD_2Cl_2 recorded at room temperature, *denotes water, $^{\#}$denotes acetone.

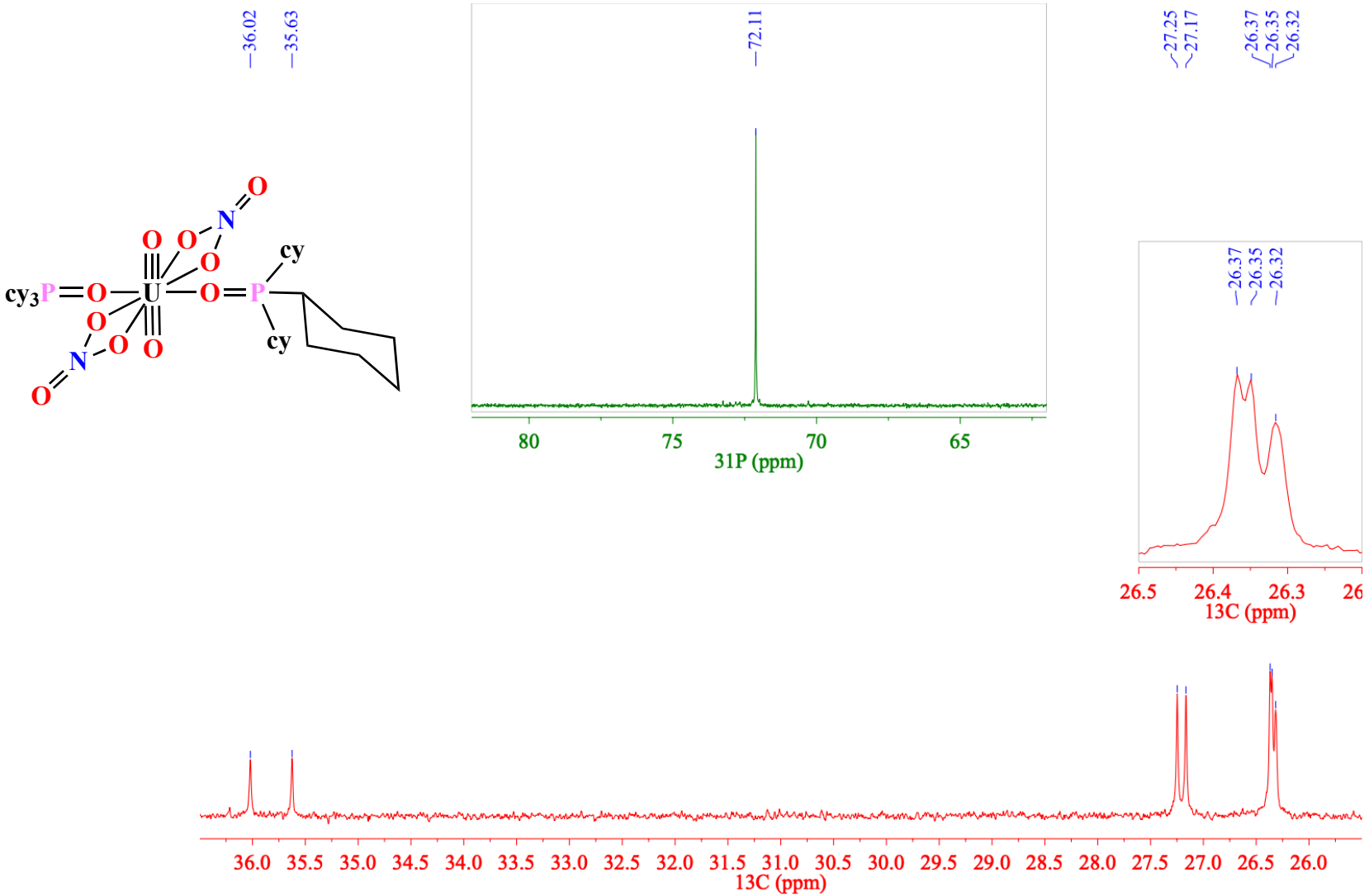

Figure S12. $^{13}C\{^{1}H\}$ (red trace) with inset of $^{31}P\{^{1}H\}$ (green trace) NMR spectra of $UO_2(NO_3)_2(OPcy_3)_2$, **3-U**, in CD_2Cl_2 recorded at room temperature. Secondary inset shows detail of splitting and overlapping resonances.

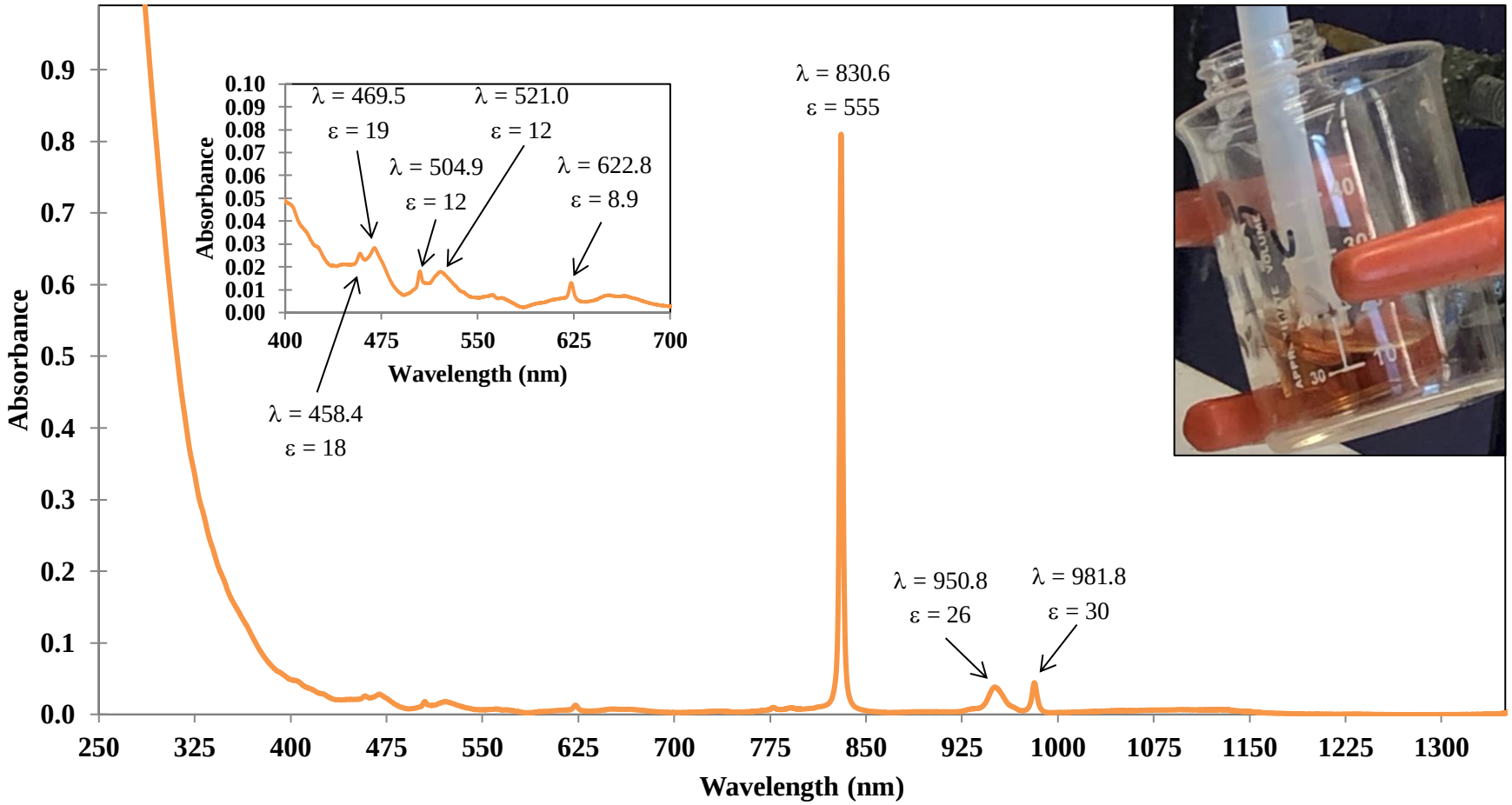

Figure S13. Solution phase UV-vis-NIR spectrum, plotted in wavelength (nm), of freshly generated $(PuO_2)^{2+}$ in $HClO_4$ (1M) at ambient temperature, with an inset showing the 400–700 nm region and a photograph of the oxidation of plutonium by ozone. The molar absorptivity was calculated based on the assumption that the excitation at λ = 830.6 nm has ε = 555 $M^{-1}L^{-1}$ taken from the literature.[31]

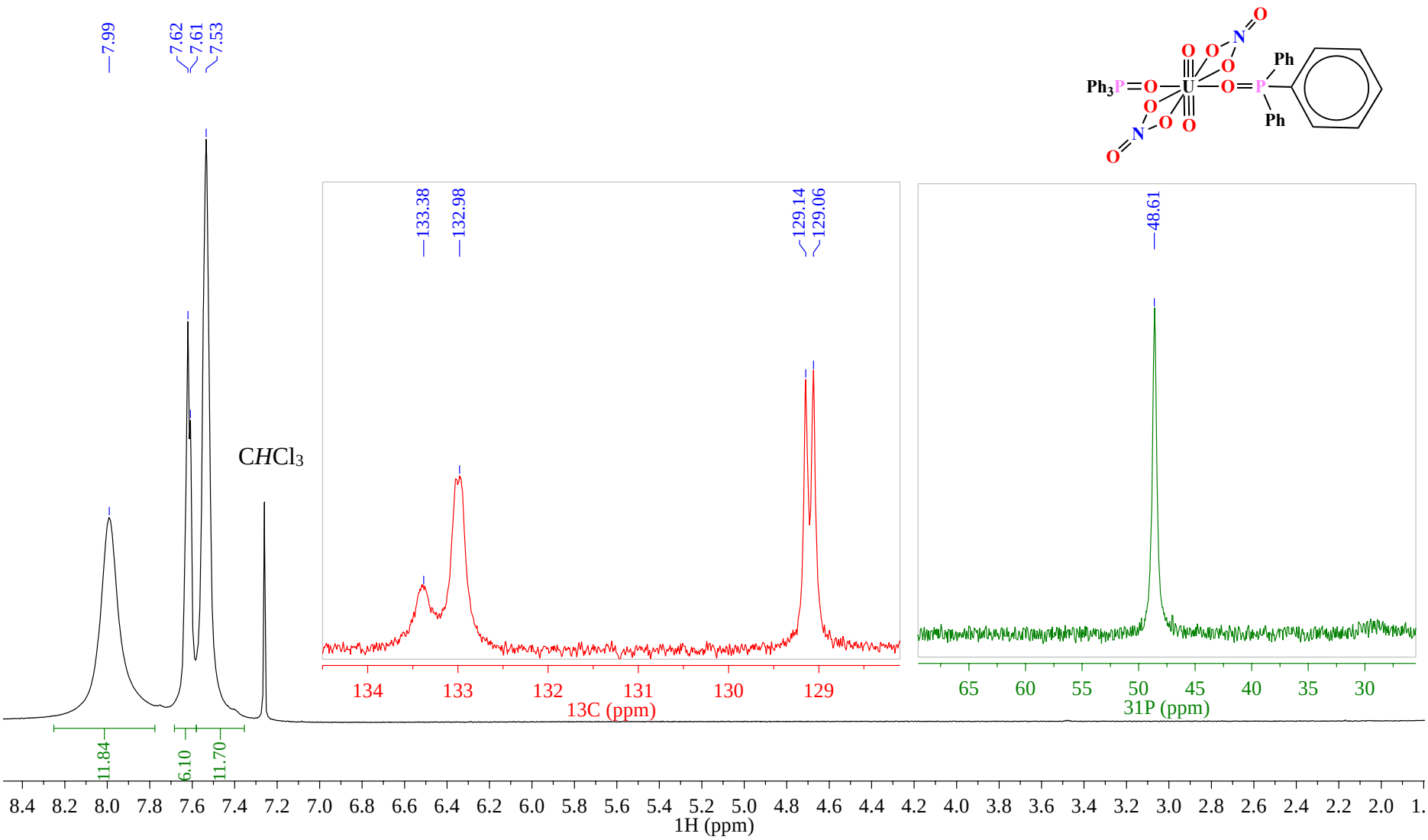

Figure S14. ^{1}H (black trace), $^{13}C\{^{1}H\}$ (red trace, inset), and $^{31}P\{^{1}H\}$ (green trace, inset) of $UO_2(NO_3)_2(OPPh_3)_2$, **4-U**, in $CDCl_3$ recorded at room temperature.

THEORETICAL CALCULATIONS

Table S3. QTAIM metrics derived from SR-CASSCF densities at the bond critical points (BCP). Electron density, ρ(r), in units of |e| $Å^{-3}$; potential, V(r), kinetic, G(r), and total energy densities, H(r), in units of kJ mol^{-1} $Å^{-3}$; whereas the covalency degree, H(r)/ρ(r), is given in kJ mol^{-1}.

	Bond	ρ(r)	δ(r)	V(r)	G(r)	H(r)	V(r)/G(r)	H(r)/ρ(r)	ε
$(AnO_2)^{2+}$	U≡O_{yl}	2.1616	1.3539	–13693.1	7918.6	–5774.5	–1.73	–2671.4	0.0000
	Pu≡O_{yl}	2.2567	1.4967	–13419.4	7408.0	–6011.3	–1.81	–2663.8	0.0000
1–U	U≡O_{yl}	1.9007	1.0827	–11393.6	6926.4	–4467.3	–1.64	–2350.3	0.0046
	U–OPcy	0.5088	0.3320	–1870.4	1724.8	–145.6	–1.08	–286.2	0.0274
	U–Cl	0.4002	0.3907	–1094.9	917.7	–177.2	–1.19	–442.8	0.0119
1–Pu	Pu≡O_{yl}	2.1190	1.2404	–12438.5	7099.2	–5339.3	–1.75	–2519.7	0.0003
	Pu–OPcy	0.4893	0.3123	–1809.0	1703.7	–105.3	–1.06	–215.2	0.0433
	Pu–Cl	0.4009	0.3875	–1115.9	947.5	–168.4	–1.18	–420.2	0.0315
ΔAn≡O_{yl}[a]	Δ U≡O_{yl}	0.2608	0.2712	–2299.4	992.2	–1307.2	–0.08	–321.1	–0.0046
	ΔPu≡O_{yl}	0.1377	0.2563	–980.8	308.8	–672.0	–0.06	–144.1	–0.0003
ΔAn–L[b]	An–OPcy	0.0196	0.0198	–61.4	21.1	–40.4	–0.02	–71.0	–0.0159
	An–Cl	–0.0007	0.0032	21.1	–29.8	–8.8	–0.02	–22.6	–0.0196

[a]Difference between metrics for the actinyl unit bonds and the actinyl phosphine oxide complex.

[b]Difference between U–L (L = OPcy, Cl) and Pu–L bonds.

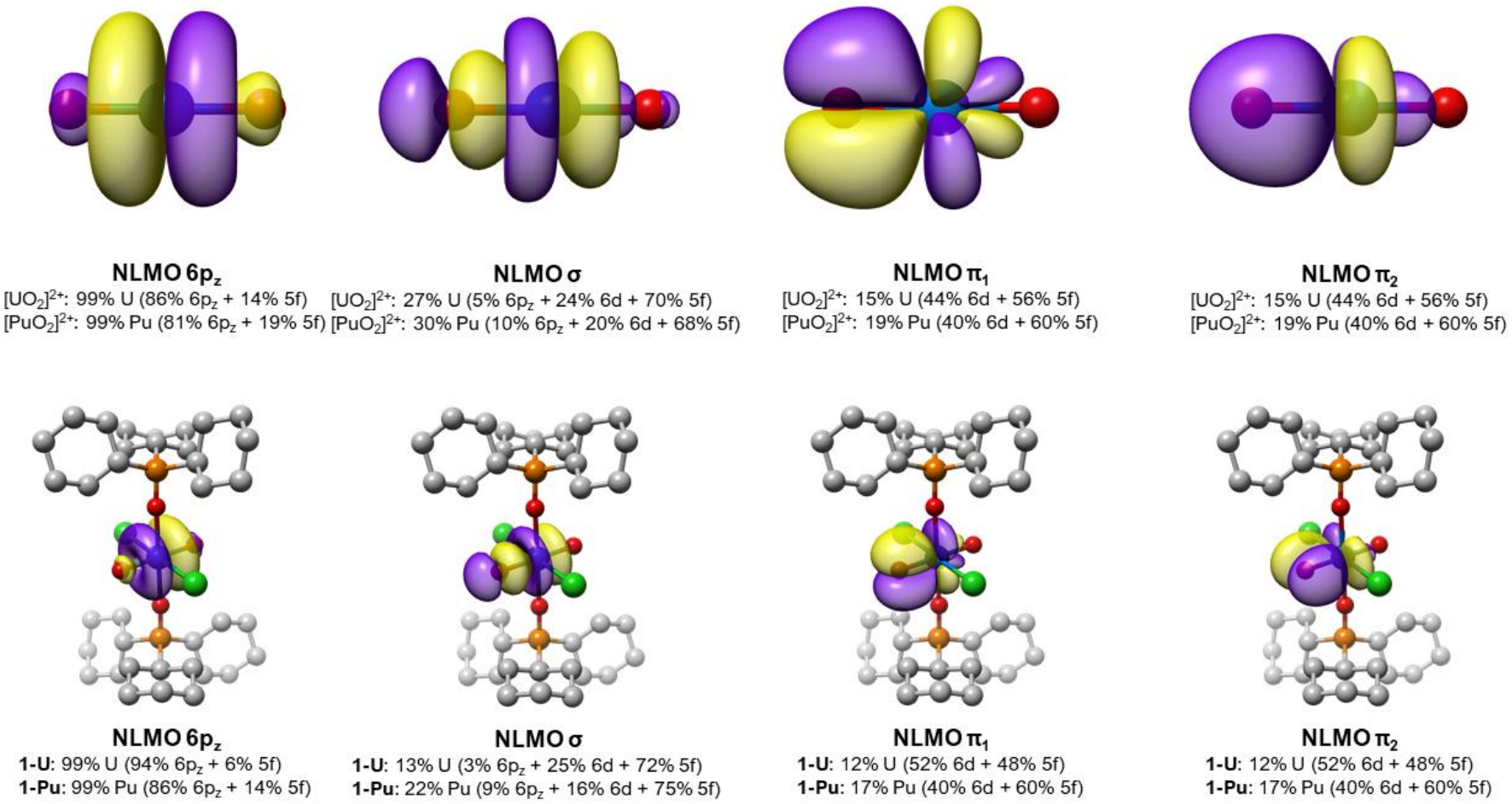

Figure S15. Selected Natural Localized Molecular Orbitals (NLMOs) describing the bonding pattern (σ and π) of $(AnO_2)^{2+}$ (above) and **1-An** (below) (An = U, Pu). The 6p_z NLMO shows how the electron density from the 6p_z semi-core orbital is polarized into the 5f shell, which is evidence of the inverse-trans influence.

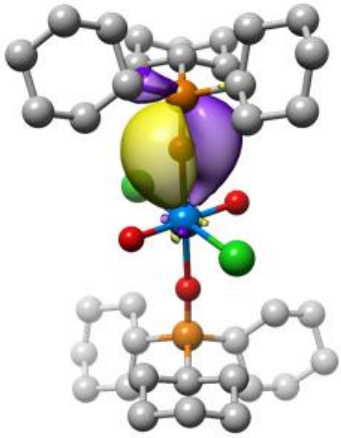

NLMO OPcy-π_1
1-U: 2% U (3% 7s + 44% 6d + 53% 5f)
1-Pu: 2% Pu (3% 7s + 33% 6d + 64% 5f)

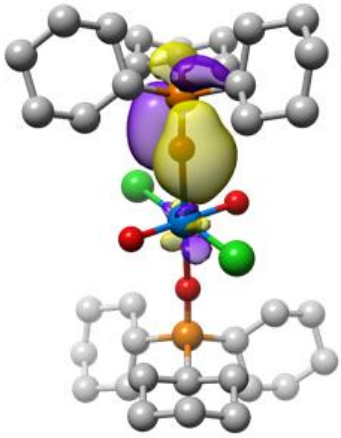

NLMO OPcy-π_2
1-U: 2% U (1% 7s + 53% 6d + 46% 5f)
1-Pu: 2% Pu (3% 7s + 52% 6d + 45% 5f)

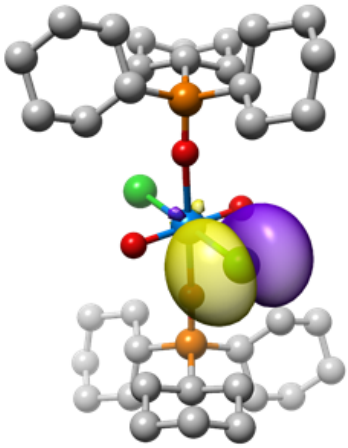

NLMO Cl-π_1
1-U: 3% U (44% 6d + 56% 5f)
1-Pu: 3% Pu (39% 6d + 61% 5f)

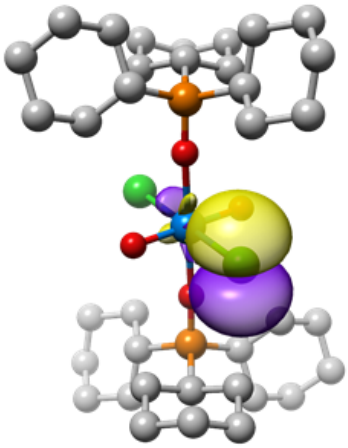

NLMO Cl-π_2
1-U: 5% U (53% 6d + 47% 5f)
1-Pu: 5% Pu (57% 6d + 43% 5f)

Figure S16. Selected NLMOs describing the π bonding pattern of the metal with the equatorial ligands in **1-U** and **1-Pu**.

Table S4. Natural Localized Molecular Orbital (NLMO) occupation number, bond order, and hybrid overlap corresponding to the axial An≡O_{yl} (An = U, Pu) bonds.

	Compound	Occupation number	Bond order contribution	Hybrid overlap
NLMO–σ	$[UO_2]^{2+}$	1.66	0.530	0.35
	1-U	1.72	0.260	0.12
	$[PuO_2]^{2+}$	1.85	0.610	0.40
	1-Pu	1.86	0.440	0.23
NLMO–$\pi_{1,2}$	$[UO_2]^{2+}$	1.85	0.300	0.52
	1-U	1.78	0.240	0.56
	$[PuO_2]^{2+}$	1.85	0.370	0.46
	1-Pu	1.85	0.330	0.56

Table S5. Natural Localized Molecular Orbital (NLMO) occupation number, bond order, and hybrid overlap corresponding to the equatorial An–L (An = U, Pu; L = OPcy, Cl) bonds.

	Compound	Occupation number	Bond order contribution	Hybrid overlap
NLMO OPcy–σ	**1-U**	2.00	0.17	0.50
	1-Pu	2.00	0.12	0.54
NLMO OPcy–π_1	**1-U**	2.00	0.03	0.47
	1-Pu	2.00	0.04	0.38
NLMO OPcy–π_2	**1-U**	2.00	0.05	0.48
	1-Pu	2.00	0.05	0.46
NLMO Cl–σ	**1-U**	2.00	0.22	0.61
	1-Pu	2.00	0.24	0.64
NLMO Cl–π_1	**1-U**	2.00	0.06	0.48
	1-Pu	2.00	0.07	0.44
NLMO Cl–π_2	**1-U**	2.00	0.09	0.48
	1-Pu	2.00	0.09	0.48

CRYSTALLOGRAPHIC DETAILS AND COMPARISONS

Table S6. Summary of crystallographic information for $PuO_2Cl_2(OPcy_3)_2$, **1-Pu**, $UO_2Cl_2(OPcy_3)_2$, **1-U**, $UO_2Cl_2(OPPh_3)_2$, **2-U**, and $UO_2(NO_3)_2(OPcy_3)_2$, **3-U**.

Compound	**1-Pu**	**1-U**	**2-U**	**3-U**
Identifier	cjw103	cjw92	cjw95	cjw91
CCDC code	2101627	2101628	2101629	2101630
Emp. Formula	$C_{36}H_{66}Cl_2O_4P_2Pu$	$C_{36}H_{66}O_4P_2Cl_2U$	$C_{36}H_{30}O_4P_2Cl_2U$	$C_{36}H_{66}N_2O_{10}P_2U$
Formula Wt.	934.82	933.75	897.47	986.87
Color	Brown	Yellow	Yellow	Yellow
Size (mm)	0.10×0.10×0.10	0.40×0.18×0.16	0.20×0.10×0.05	0.32×0.14×0.10
Temp (K)	100(2)	120(2)	170(2)	100(2)
Crystal System	Triclinic	Triclinic	Monoclinic	Monoclinic
Space Group	$P\bar{1}$	$P\bar{1}$	$P2_1$	$P2_1/n$
***a* (Å)**	8.7416(4)	8.7605(2)	10.0387(6)	8.5735(6)
***b* (Å)**	14.1281(7)	14.1151(4)	18.654(1)	16.444(1)
***c* (Å)**	17.1398(8)	17.1633(5)	10.7043(6)	14.6892(9)
***α* (°)**	69.306(4)	69.441(3)	90	90
***β* (°)**	89.512(4)	89.371(2)	117.802(2)	103.075(6)
***γ* (°)**	76.786(4)	77.147(2)	90	90
Volume (Å^3)	1921.7(2)	1932.1(1)	1773.1(2)	2017.2(2)
Z	2	2	2	2
ρ_{calcd} (Mg/m^3)	1.621	1.605	1.681	1.625
μ (mm^{-1})	1.973	4.457	4.855	4.158
F(000)	944	940	868	996
Θ range (°)	1.588 to 25.681	1.639 to 25.680	2.151 – 27.607	1.887 – 25.682
Index Range	$-10 \le h \le 10$, $-17 \le k \le 17$, $-20 \le l \le 20$	$-10 \le h \le 9$, $-17 \le k \le 17$, $-20 \le l \le 20$	$-13 \le h \le 13$, $-24 \le k \le 24$, $-13 \le l \le 13$	$-10 \le h \le 10$, $-20 \le k \le 20$, $-17 \le l \le 17$
Refl. Collected	87287	35033	28492	24252

Indept. Refl. [R(int)]	7198 [0.1237]	7307 [0.0497]	8125 [0.0420]	3807 [0.1389]
Complet. (%)	98.5	99.5	100.0	99.3
Max/Min Trans.	1.0000 / 0.7199	1.0000 / 0.4832	0.7456 / 0.4809	1.0000 / 0.2937
Data / Restraints / Par	7198 / 0 / 409	7307 / 6 / 409	8125 / 1 / 407	3807 / 0 / 232
GOOF	0.877	0.911	1.033	0.900
R1[a] [$I > 2.0\sigma$(I)]	0.0399	0.0270	0.0278	0.0399
wR2 (all data)	0.0829	0.0549	0.0651	0.0851
Peak/Hole (e^{-}Å^{-3})	2.231 / −1.398	1.081 / −0.953	1.791 / −0.694	1.770 / −1.415
BASF			0.055(7)	

[a]Definitions: R1 = $\Sigma||F_o| - |F_c||/\Sigma|F_o|$, wR2 = $[\Sigma w(F_o^2 - F_c^2)^2/\Sigma w(F_o^2)^2]^{1/2}$.

Goof = S = $[\Sigma[w(F_o^2\text{-}F_c^2)^2] / (n\text{-}p)]^{1/2}$ where n is the number of reflections and p is the total number of parameters refined.

Details of Crystallographic Collections, Refinement, Molecular Plots, Relevant Bond Metric Tables, and Bond Metric Comparison Tables.

$PuO_2Cl_2(OPcy_3)_2$, 1-Pu, an irregular brown crystal of approximate dimensions 0.10 × 0.10 × 0.10 mm was mounted on a cryoloop and transferred to the diffractometer A calculated scan with 45 sec exposure/frame was utilized to collect the data at a temperature of 100(2) K. There were no systematic absences or any diffraction symmetry other than the Friedel condition. The centrosymmetric triclinic space group $P\bar{1}$ was assigned and later determined to be correct. The structure was solved as a multicomponent twin.

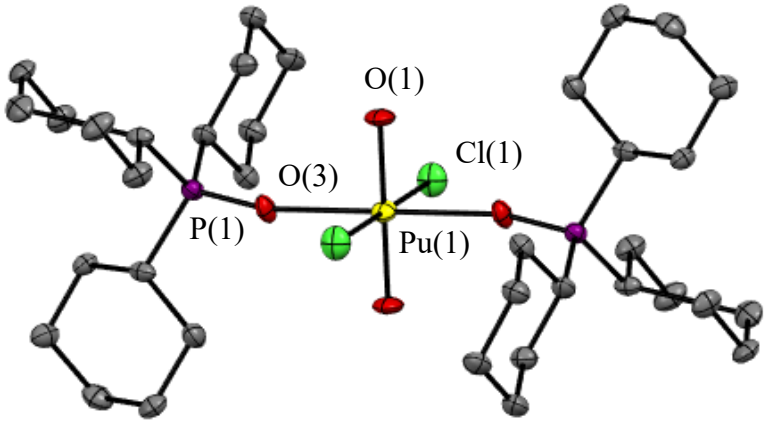

Figure S17. Thermal ellipsoid plot of one crystallographically independent unit of $PuO_2Cl_2(OPcy_3)_2$, **1-Pu**, drawn at the 50% probability level with hydrogen atoms omitted for clarity, only non-carbon atoms in the asymmetric unit are labeled.

Table S7. Relevant bond lengths [Å] and angles [°] for **$PuO_2Cl_2(OPcy_3)_2$, 1-Pu**.

Pu(1)-Cl(1)	2.633(2)	Pu(2)-Cl(2)	2.652(2)
Pu(1)-O(1)	1.762(4)	Pu(2)-O(2)	1.742(4)
Pu(1)-O(3)	2.301(4)	Pu(2)-O(4)	2.281(5)
P(1)-O(3)	1.510(5)	P(2)-O(4)	1.503(5)
Cl(1)-Pu(1)-Cl(1)#1	180.0	Cl(2)#2-Pu(2)-Cl(2)	180.0
O(1)-Pu(1)-Cl(1)	87.9(2)	O(2)-Pu(2)-Cl(2)	89.4(1)
O(1)-Pu(1)-Cl(1)#1	92.1(2)	O(2)-Pu(2)-Cl(2)#2	90.7(1)
O(1)-Pu(1)-O(1)#1	180.0	O(2)#2-Pu(2)-O(2)	180.0(4)
O(1)-Pu(1)-O(3)	90.1(2)	O(2)-Pu(2)-O(4)	89.8(2)
O(1)-Pu(1)-O(3)#1	89.9(2)	O(2)-Pu(2)-O(4)#2	90.2(2)
O(3)-Pu(1)-Cl(1)	89.4(1)	O(4)-Pu(2)-Cl(2)#2	91.1(1)
O(3)-Pu(1)-Cl(1)#1	90.6(1)	O(4)-Pu(2)-Cl(2)	88.9(1)
O(3)#1-Pu(1)-O(3)	180.0	O(4)-Pu(2)-O(4)#2	180.0(1)
P(1)-O(3)-Pu(1)	167.1(3)	P(2)-O(4)-Pu(2)	172.2(3)

Symmetry transformations used to generate equivalent atoms:

#1 −x, −y + 1, −z + 1 #2 −x + 1, −y + 1, −z + 2

Table S8. Bond Metric Comparisons of $PuO_2Cl_2(OPR_3)_2$, (R = Ph, cy).

	$PuO_2Cl_2(OPPh_3)_2$[32]	**$PuO_2Cl_2(OPcy_3)_2$†**
Pu–O_{yl} (Å)	1.747(4)	1.762(4); 1.742(4)
Pu–O_P (Å)	2.302(4)	2.301(4); 2.281(5)
Pu–Cl (Å)	2.630(2)	2.633(2); 2.652(2)
O–P (Å)	1.505(4)	1.510(5); 1.503(5)
O_{yl}–Pu–O_{yl} (°)	180	180; 180
O_p–Pu–O_p (°)	180	180; 180
Pu–O_p–P (°)	159.9(2)	167.1(3); 172.2(3)
Cl–Pu–Cl (°)	180	180; 180

†Contains two half molecules in the asymmetric unit; O_{yl} represents the "yl" oxo; O_p represents the phosphine oxide

$UO_2Cl_2(OPcy_3)_2$, 1-U, a yellow plate crystal of approximate dimensions 0.40 × 0.18 × 0.16 mm was mounted on a cryoloop and transferred to the diffractometer A calculated scan with 10 sec exposure/frame was utilized to collect the data set at a temperature of 120(2) K. There were no systematic absences or any diffraction symmetry other than the Friedel condition. The centrosymmetric triclinic space group $P\bar{1}$ was assigned and later determined to be correct. The same complex is known under CCDC code CIGCEB which features a lattice DCM.[30] C9 could not be satisfactorily refined and was modeled to be approximately isotropic (ISOR).

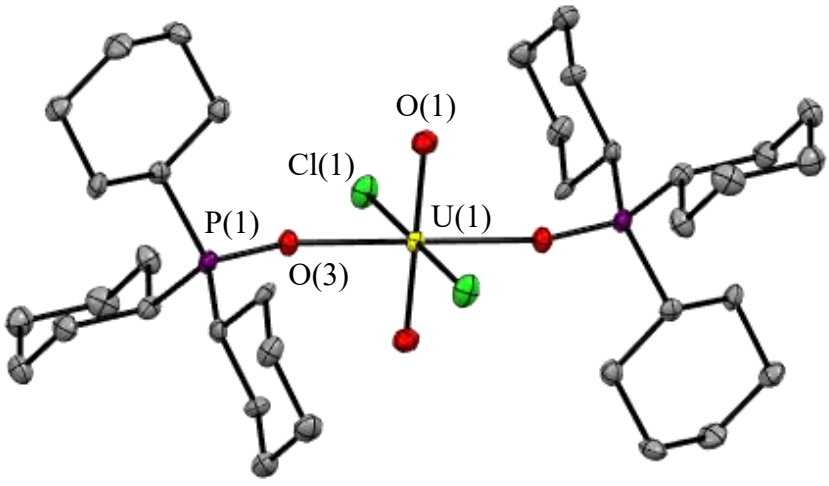

Figure S18. Thermal ellipsoid plot of one crystallographically independent unit of $UO_2Cl_2(OPcy_3)_2$, **1-U**, drawn at the 50% probability level with hydrogen atoms omitted for clarity, only non-carbon atoms in the asymmetric unit are labeled.

Table S9. Relevant bond lengths [Å] and angles [°] for **$UO_2Cl_2(OPcy_3)_2$, 1-U**.

U(1)-Cl(1)	2.660(1)	U(2)-Cl(2)	2.670(1)
U(1)-O(1)	1.760(3)	U(2)-O(2)	1.767(3)
U(1)-O(3)	2.299(3)	U(2)-O(4)	2.279(3)
P(1)-O(3)	1.519(3)	P(2)-O(4)	1.517(3)
Cl(1)#1-U(1)-Cl(1)	180.0	Cl(2)-U(2)-Cl(2)#2	180.0
O(1)#1-U(1)-Cl(1)#1	88.4(1)	O(2)#2-U(2)-Cl(2)#2	89.8(1)
O(1)-U(1)-Cl(1)	88.4(1)	O(2)-U(2)-Cl(2)	89.8(1)
O(1)#1-U(1)-Cl(1)	91.6(1)	O(2)-U(2)-Cl(2)#2	90.2(1)
O(1)-U(1)-Cl(1)#1	91.6(1)	O(2)#2-U(2)-Cl(2)	90.2(1)
O(1)#1-U(1)-O(1)	180.0	O(2)-U(2)-O(2)#2	180.0
O(1)#1-U(1)-O(3)	90.2(1)	O(2)#2-U(2)-O(4)	89.8(1)
O(1)#1-U(1)-O(3)#1	89.8(1)	O(2)-U(2)-O(4)#2	89.8(1)
O(1)-U(1)-O(3)	89.8(1)	O(2)#2-U(2)-O(4)#2	90.2(1)
O(1)-U(1)-O(3)#1	90.2(1)	O(2)-U(2)-O(4)	90.2(1)
O(3)#1-U(1)-Cl(1)	89.68(8)	O(4)#2-U(2)-Cl(2)	91.11(7)
O(3)-U(1)-Cl(1)#1	89.68(8)	O(4)-U(2)-Cl(2)	88.89(7)
O(3)-U(1)-Cl(1)	90.32(8)	O(4)#2-U(2)-Cl(2)#2	88.90(7)
O(3)#1-U(1)-Cl(1)#1	90.32(8)	O(4)-U(2)-Cl(2)#2	91.11(7)
O(3)#1-U(1)-O(3)	180.0	O(4)-U(2)-O(4)#2	180.0
P(1)-O(3)-U(1)	168.0(2)	P(2)-O(4)-U(2)	172.3(2)

Symmetry transformations used to generate equivalent atoms:

#1 −x, −y + 1, −z + 1 #2 −x + 1, −y + 1, −z + 2

Table S10. Bond Metric Comparisons of $UO_2Cl_2(OPcy_3)_2$, **1-U**, with previous report.

	$UO_2Cl_2(OPcy_3)_2$•$2CH_2Cl_2$[30]	**$UO_2Cl_2(OPcy_3)_2$**†
U–O_{yl} (Å)	1.778(5)	1.760(3); 1.767(3)
U–O_p (Å)	2.278(5)	2.299(3); 2.279(3)
U–Cl (Å)	2.667(2)	2.660(1); 2.670(1)
O–P (Å)	1.535(5)	1.519(3); 1.517(3)
O_{yl}–U–O_{yl} (°)	179.6(3)	180; 180
O_p–U–O_p (°)	179.7(2)	180; 180
U–O_p–P (°)	167.3(3)	168.0(2); 172.3(2)
Cl–U–Cl (°)	179.89(7)	180; 180

†Contains two half molecules in the asymmetric unit; O_{yl} represents the "yl" oxo; O_p represents the phosphine oxide

$UO_2Cl_2(OPPh_3)_2$, 2-U, a yellow plate crystal of approximate dimensions 0.07 × 0.15 × 0.22 mm was mounted on a cryoloop and transferred to the diffractometer. Unit cell analysis showed that the compound is known under the structure code CDXUPO01,[33] which was published in the $B2_1$ space group and recorded at room temperature. The structure is also known in the $P\bar{1}$ space group under structure code CDXUPO and also recorded at room temperature.[34] To obtain an improved refinement a low temperature collection was performed. A 15 sec exposure/frame with a scan width of 0.3° was utilized to collect a hemi sphere of data with a detector distance of 35 mm at a temperature of 170(2) K. Attempts to collect data at 120 or 150 K led to crystal cracking. The diffraction symmetry was 2/*m* and the systematic absences were consistent with the monoclinic space groups $P2_1$ and $P2_1/m$. It was later determined that space group $P2_1$ was correct. The structure was refined as an inversion twin with ambiguous results giving a BASF value of 0.055(7).

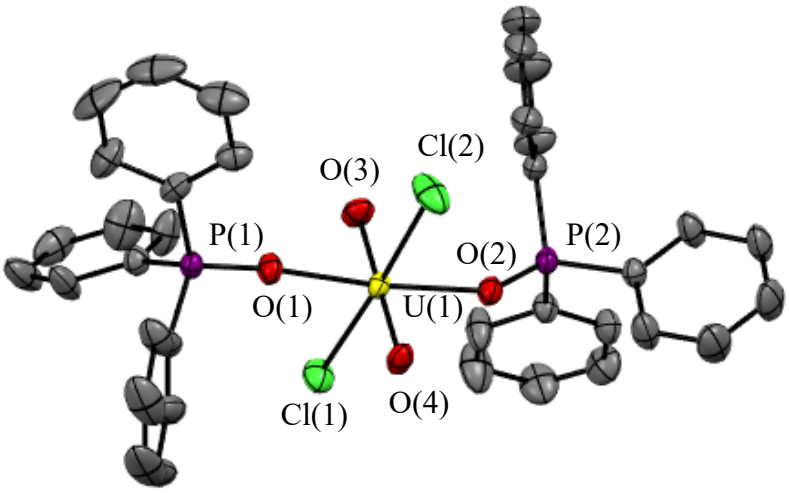

Figure S19. Thermal ellipsoid plot of $UO_2Cl_2(OPPh_3)_2$, **2-U**, drawn at the 50% probability level with hydrogen atoms omitted for clarity.

Table S11. Relevant bond lengths [Å] and angles [°] for $UO_2Cl_2(OPPh_3)_2$, **2-U**.

U(1)-Cl(1)	2.661(2)	U(1)-O(3)	1.765(5)
U(1)-Cl(2)	2.640(2)	U(1)-O(4)	1.772(5)
U(1)-O(1)	2.292(5)	P(1)-O(1)	1.507(5)
U(1)-O(2)	2.302(5)	P(2)-O(2)	1.513(5)
Cl(2)-U(1)-Cl(1)	176.55(7)	O(3)-U(1)-O(2)	91.6(2)
O(1)-U(1)-Cl(1)	90.4(1)	O(3)-U(1)-O(4)	179.0(2)
O(1)-U(1)-Cl(2)	86.2(1)	O(4)-U(1)-Cl(1)	89.4(2)
O(1)-U(1)-O(2)	174.8(2)	O(4)-U(1)-Cl(2)	90.1(2)
O(2)-U(1)-Cl(1)	93.5(1)	O(4)-U(1)-O(1)	88.8(2)
O(2)-U(1)-Cl(2)	89.8(1)	O(4)-U(1)-O(2)	87.8(2)
O(3)-U(1)-Cl(1)	89.8(2)	P(1)-O(1)-U(1)	167.1(3)
O(3)-U(1)-Cl(2)	90.7(2)	P(2)-O(2)-U(1)	151.4(3)
O(3)-U(1)-O(1)	91.8(2)		

Table S12. Bond Metric Comparisons of $UO_2Cl_2(OPPh_3)_2$, **2-U**, with previous reports.

	1978 Report[34]	**1991 Report[33]**	**This Report**
U–O_{yl} (Å)	1.764(9)	1.753(12); 1.767(12)	1.765(5); 1.772(5)
U–O_p (Å)	2.300(8)	2.306(12); 2.339(12)	2.292(5); 2.302(5)
U–Cl (Å)	2.645(5)	2.673(4); 2.657(4)	2.661(2); 2.640(2)
O–P (Å)	1.518(8)	1.535(3); 1.4677(12)	1.507(5); 1.513(5)
O_{yl}–U–O_{yl} (°)	180	178.6(6)	179.0(2)
O_p–U–O_p (°)	180	175.3(4)	174.8(2)
U–O_p–P (°)	158.7(6)	166.2(8); 151.7(8)	167.1(3); 151.4(3)
Cl–U–Cl (°)	180	175.3(4)	176.55(7)

†Contains two half molecules in the asymmetric unit; O_{yl} represents the "yl" oxo; O_p represents the phosphine oxide

$UO_2(NO_3)_2(OPcy_3)_2$, 3-U, a yellow crystal of approximate dimensions 0.10 × 0.14 × 0.32 mm was mounted on a cryoloop, and transferred to the diffractometer. A 20 sec exposure/frame along with a 0.4° scan width was utilized to collect a hemi-sphere of data with the detector at a distance 50 mm at a temperature of 100(2) K. The centrosymmetric monoclinic space group $P2_1/n$ was assigned and determined to be correct.

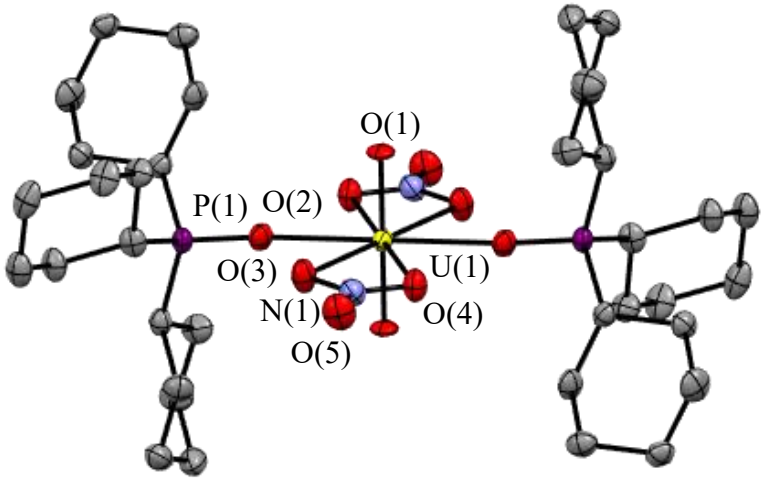

Figure S20. Thermal ellipsoid plot of $UO_2(NO_3)_2(OPcy_3)_2$, **3-U**, drawn at the 50% probability level with hydrogen atoms omitted for clarity, only heteroatoms in the asymmetric unit are labeled.

Table S13. Relevant bond lengths [Å] and angles [°] for $UO_2(NO_3)_2(OPcy_3)_2$, **3-U**.

U(1)-O(1)	1.768(3)	U(1)-O(4)	2.552(4)
U(1)-O(2)	2.336(4)	P(1)-O(2)	1.512(4)
U(1)-O(3)	2.541(4)		
O(1)#1-U(1)-O(1)	180.0	O(2)-U(1)-O(3)	64.8(1)
O(1)-U(1)-O(2)#1	88.8(1)	O(2)-U(1)-O(4)#1	65.6(1)
O(1)-U(1)-O(2)	91.2(1)	O(2)-U(1)-O(4)	114.4(1)
O(1)#1-U(1)-O(3)	91.6(1)	O(3)-U(1)-O(3)#1	180.00(9)
O(1)-U(1)-O(3)	88.4(1)	O(3)#1-U(1)-O(4)	130.3(1)
O(1)-U(1)-O(4)#1	89.9(1)	O(3)-U(1)-O(4)	49.7(1)
O(1)-U(1)-O(4)	90.2(1)	O(3)-U(1)-O(4)#1	130.3(1)
O(2)#1-U(1)-O(2)	180.0	O(4)-U(1)-O(4)#1	180.0
O(2)#1-U(1)-O(3)	115.2(1)	P(1)-O(2)-U(1)	175.8(2)

Symmetry transformations used to generate equivalent atoms:

#1 –x + 1, –y + 1, –z + 1

Table S14. Bond Metric Comparisons of $UO_2(NO_3)_2(OPcy_3)_2$, **3-U**, with $UO_2(NO_3)_2(OPPh_3)_2$, **4-U**, from the literate.

	$UO_2(NO_3)_2(OPPh_3)_2$[35]	**$UO_2(NO_3)_2(OPcy_3)_2$**
U–O_{yl} (Å)	1.764(9)	1.768(3)
U–O_N (Å)	2.524(7); 2.536(11)	2.541(4); 2.552(4)
U–O_p (Å)	2.359	2.336(4)
O–P (Å)	1.505(9)	1.512(4)
O_{yl}–U–O_{yl} (°)	180	180
O_p–U–O_p (°)	180	180
U–O_p–P (°)	160.0(4)	175.8(2)

"O_{yl}" represents the uranyl-oxo oxygen; O_N represents the nitrate oxygen; O_p represents the phosphine oxide oxygen

REFERENCES

1. F. J. Arnaiz and C. J. Burns, in *Inorg. Synth.*, ed. D. Coucouvanis, John Wiley & Sons, Inc., 2002, vol. 33, ch. 4, pp. 204-206.
2. J. I. Bullock, *J. Inorg. Nucl. Chem.*, 1967, **29**, 2257-2264.
3. E. Veerashekhar Goud, B. B. Pavan Kumar, Y. Shruthi, A. Paul, A. Sivaramakrishna, K. Vijayakrishna, C. V. S. Brahmananda Rao, K. N. Sabharwal and H. S. Clayton, *J. Coord. Chem.*, 2013, **66**, 2647-2658.
4. J. P. Day and L. M. Venanzi, *J. Chem. Soc.*, 1966, 1363-1367.
5. A. Bractecki and D. Dembicka, *Inorg. Chim. Acta*, 1969, **3**, 59-64.
6. M. P. Redmond, S. M. Cornet, S. D. Woodall, D. Whittaker, D. Collison, M. Helliwell and L. S. Natrajan, *Dalton Trans.*, 2011, **40**, 3914-3926.
7. E. Hashem, T. McCabe, C. Schulzke and R. J. Baker, *Dalton Trans.*, 2014, **43**, 1125-1131.
8. G. R. Fulmer, A. J. M. Miller, N. H. Sherden, H. E. Gottlieb, A. Nudelman, B. M. Stoltz, J. E. Bercaw and K. I. Goldberg, *Organometallics*, 2010, **29**, 2176-2179.
9. APEX3 (2018.7-2), Madison, WI, 2018.
10. CrysAlisPRO, version 39.27b; Oxfor Diffraction/Agilent Technologies UK Ltd: Yarnton, U.K., 2017
11. G. M. Sheldrick, *Acta Cryst.*, 2015, **A71**, 3-8.
12. G. M. Sheldrick, *Acta Cryst.* , 2015, **C71**, 3-8.
13. International Tables for X-Ray Crystallography 1992, Vol. C., Dordrecht: Kluwer Academic Publishers.
14. C. Adamo and V. Barone, *J. Chem. Phys.*, 1999, **110**, 6158-6170.
15. F. Weigend and R. Ahlrichs, *Phys. Chem. Chem. Phys.*, 2005, **7**, 3297-3305.
16. D. A. Pantazis and F. Neese, *J. Chem. Theory Comput.*, 2011, **7**, 677-684.
17. B. A. Hess, *Phys. Rev. A*, 1986, **33**, 3742-3748.
18. G. te Velde, F. M. Bickelhaupt, E. J. Baerends, C. Fonseca Guerra, S. J. A. van Gisbergen, J. G. Snijders and T. Ziegler, *J. Comput. Chem.*, 2001, **22**, 931-967.
19. E. v. Lenthe, E. J. Baerends and J. G. Snijders, *J. Chem. Phys.*, 1993, **99**, 4597-4610.
20. B. O. Roos, P. R. Taylor and P. E. M. Sigbahn, *Chem. Phys.*, 1980, **48**, 157-173.
21. C. Angeli, R. Cimiraglia and J.-P. Malrieu, *J. Chem. Phys.*, 2002, **117**, 9138-9153.
22. F. Neese, *WIREs Comput. Mol. Sci.*, 2018, **8**, e1327.
23. R. F. W. Bader, *Atoms in Molecules*, Oxford University Press, Oxford, 1994.

24. AIMAll (Version 19.10.12), Keith, T. A., TK Gristmill Software, Overland Park KS, USA, 2019, aim.tkgristmill.com.
25. A. E. Reed and F. Weinhold, *J. Chem. Phys.*, 1985, **83**, 1736-1740.
26. A. E. Reed, L. A. Curtiss and F. Weinhold, *Chem. Rev.*, 1988, **88**, 899-926.
27. E. D. Glendening, A. E. Badenhoop, A. E. Reed, J. E. Carpenter, J. A. Bohmann, C. M. Morales, P. Karafiloglou, C. R. Landis and F. Weinhold, *Journal*, 2018.
28. S. M. Cornet, I. May, M. J. Sarsfield, N. Kaltsoyannis, J. Haller, C. D. Auwer and D. Meyer, *J. Alloys Comp.*, 2007, **444–445**, 453-456.
29. Due to apparent Pu^{4+} impurities ε values cannot be given, see spectra for details
30. L. J. L. Häller, N. Kaltsoyannis, M. J. Sarsfield, I. May, S. M. Cornet, M. P. Redmond and M. Helliwell, *Inorg. Chem.*, 2007, **46**, 4868-4875.
31. D. L. Clark, S. S. Hecker, G. D. Jarvinen and M. P. Neu, in *The Chemistry of the Actinide and Transactinide Elements*, eds. L. R. Morss, N. M. Edelstein and J. Fuger, Springer Netherlands, Dordrecht, 2006, pp. 813-1264.
32. C. Berthon, N. Boubals, I. A. Charushnikova, D. Collison, S. M. Cornet, C. Den Auwer, A. J. Gaunt, N. Kaltsoyannis, I. May, S. Petit, M. P. Redmond, S. D. Reilly and B. L. Scott, *Inorg. Chem.*, 2010, **49**, 9554-9562.
33. S. B. Akona, J. Fawcett, J. H. Holloway, D. R. Russell and I. Leban, *Acta Cryst.*, 1991, **C47**, 45-48.
34. G. Bombieri, E. Forsellini, J. P. Day and W. I. Azeez, *Dalton Trans.*, 1978, 677-680.
35. N. W. Alcock, M. M. Roberts and D. Brown, *Dalton Trans.*, 1982, 25-31.